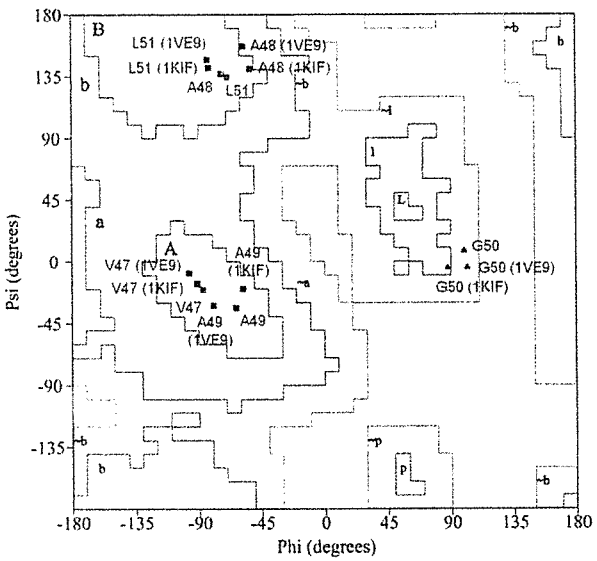

Figure 6. φ/ψ plots of the hydrophobic stretch (residues 47–51) of human (green) and porcine (red; PDB codes 1KIF, 1VE9) DAO-benzoate structures. The φ/ψ combinations of Ala48, Ala49, and Gly50 are diversified among the three structures, while those of Val47 and Leu51 are conserved. [A, B, L] most favored regions; [a, b, l, p] additional allowed regions; [~a, ~b, ~l, ~p] generously allowed regions.

was heated at 59°C for 3 min and then rapidly cooled to <10°C in an ice-water bath. The denatured proteins were removed by centrifugation, and the supernatant was precipitated with 70% ammonium sulfate. After dialysis overnight against buffer A (10 mM Tris-HCl at pH 8.0, 125 mM KCl, 10 μM FAD, 200 μM Na benzoate, and 4.5 μg/mL PMSF) followed by centrifugation, the supernatant was applied to an anion-exchange DEAE Sepharose CL-6B (Sigma) column (3 × 30 cm) equilibrated with buffer A without FAD, and the column eluate was fractionated. Yellow fractions, which contained the DAO holoenzyme, were detected based on the OD_{455}/OD_{280} ratio and SDS-PAGE, then pooled and precipitated with 70% ammonium sulfate. After dialysis overnight against buffer B (50 mM Na phosphate at pH 6.8, 10 μM FAD, and 200 μM Na benzoate) followed by centrifugation, the supernatant was applied to a hydroxylapatite (nacalai) column (1 × 50 cm) equilibrated with buffer B without FAD, and the column eluate was fractionated. Again, the yellow fractions were detected based on the OD_{455}/OD_{280} ratio and SDS-PAGE, pooled, and precipitated with 70% ammonium sulfate. The resultant purified protein was confirmed as a single band on SDS-PAGE (Fig. 1B). Protein concentrations were determined with a BCA Protein Assay Kit (Pierce) using BSA as a standard, or for the purified DAO, using an extinction coefficient previously obtained with porcine DAO (11.3 $mM^{-1}cm^{-1}$ at 455 nm). The N-terminal 10 residues of the purified enzyme were confirmed by protein sequencing.

Kinetic analyses

DAO activity was measured in oxygraphic assays using a modification of the method used to characterize recombinant porcine DAO (Miyano et al. 1991). A Clark oxygen electrode (Gilson, model 5/6 Oxygraph) was used for the assays. The standard reaction mixture contained DAO and 50 μM FAD in a total volume of 1.8 mL. The reactions were initiated by the addition of DAO and carried out in 50 mM Na pyrophosphate buffer (pH 8.3) at 25°C. The Michaelis constant (K_m) and turnover number (k_{cat}) were estimated from double reciprocal plots of the initial velocity versus the substrate concentration (Table 1B). The inhibition constant (K_i) for benzoate was estimated from double reciprocal plots of the initial velocity versus the D-Pro concentration in the presence of benzoate (0–20 μM) (Table 1B).

Crystallization

The ammonium sulfate precipitant of the purified enzyme was dialyzed overnight against buffer containing 10 mM Na citrate (pH 8.0), 20 μM FAD, and 400 μM Na benzoate at 4°C, and then concentrated to 10 mg/mL. Crystallization conditions were screened using the hanging-drop vapor diffusion method. Yellow crystals were obtained from polyethylene glycol (PEG) 4000, ammonium acetate, and Na citrate (pH 8.0) at 20°C. Further screening resulted in single crystals after mixing 2 μL of protein sample (10 mg/mL) with the same volume of the reservoir solution (10% [w/v] PEG 4000, 0.2 M ammonium acetate, 0.1 M Na citrate at pH 8.0, and 12% [v/v] glycerol). The 12% (v/v) glycerol enhanced the crystal quality. Crystals grew to an average size of 0.1 × 0.1 × 0.05 mm in 10 d (Fig. 1C).

Data collection

The data collection statistics are summarized in Table 2. Using KEK Bl5a at the Photon Factory (Tsukuba, Japan), the native data were collected at 2.5 Å resolution using monochromatized radiation at λ = 1.0 Å and a ADSC Quantum 315 CCD detector. The distance between the crystal and detector was 350 mm, and the scan angle was 1.0°. Data were processed using the HKL2000 software package (Otwinowski and Minor 1997).

Structural determination and refinement

The refinement statistics are summarized in Table 3. Structural determination and refinement calculations were carried out

Table 2. *Data collection statistics*

Unit cell (Å)	a = 150.976, b = 183.184, c = 51.075
Space group	$P2_12_12$
Beamline	KEK BL-5A
Wavelength (Å)	1.0
Detector (type)	CCD (ADSC Quantum 315)
Temperature (K)	100.0
Oscillation angle (°)	1
No. of images	180
Resolution (Å)	50.00–2.50 (2.59–2.50)
No. of reflections (observed)	49,644 (4877)
Completeness (%)	99.5 (99.8)
R-merge I (observed)	0.077 (0.377)
I/σ	13.4
Redundancy	5.8 (5.5)
Solvent content (%)	44.91
Matthews coefficient ($Å^3$/Da)	2.23
No. of subunits per asymmetric unit	4

Values in parentheses are for the highest resolution shell.

Table 3. *Refinement statistics*

Resolution (Å)	116.25–2.50 (2.57–2.50)
No. of reflections (observed)	47,032
No. of reflections (R-free)	2,516
R-work (%)	22.3
R-free (%)	27.0
No. of nonhydrogen atoms	
Protein	10,932
FAD	212
Benzoate	36
Water	256
Average B factors (Å^2)	
Overall	51.861
Protein atoms	52.229
FAD atoms	39.029
Benzoate atoms	60.289
Water molecules	45.611
RMS deviations	
Bond lengths (Å)	0.012
Bond angles (°)	1.384
Residues in Ramachandran plot (%)	
Most favored	87.7
Additionally allowed	12.3
Generously allowed	0.0
Disallowed	0.0

using the CCP4 suite (Collaborative Computational Project, Number 4 1994). The structure was solved by molecular replacement using MOLREP with the porcine DAO dimer (Miura et al. 1997) serving as the search model. The rotation function and the translation function clearly identified the positions of two DAO dimers (Rfac = 0.543/Correlation coefficient = 0.551). Model building was carried out manually using XTALVIEW. FAD and benzoate were built into the difference electron density using strict noncrystallographic symmetry. Since the former data (2.4 Å) have a low degree of completeness (92.7% [85.0%]), we refined the model against other 2.5 Å data. However, both structures were basically the same and included the same conformation of the VAAGL hydrophobic stretch. Refinement was carried out using Refmac5 (Murshudov et al. 1997) and CNS (Brünger et al. 1998). SIGMAA-weighted maps calculated with coefficients $2F_o$–F_c and F_o–F_c were used for the model rebuilding. The final model consists of residues 1–340 for each of the four DAO subunits. Water molecules with thermal factors >70 Å^2 after refinement were excluded from the list. After the final round of refinement, the stereochemistry of the structure was assessed with PROCHECK, taking particular care of the conformation of the hydrophobic stretch. The conformation was confirmed by an omit map using a simulated annealing method after omitting the VAAGL hydrophobic stretch.

Acknowledgments

We thank Nobuhiko Katunuma and Kenji Aki for discussions; Hisaaki Taniguchi, Kazuko Fujiwara, and Kazuko Okamura-Ikeda for discussions on crystallization conditions; and Ritsu Chounan for help with the protein sequencing. H.T. thanks Masamichi Ikeguchi (Department of Bioinformatics, Faculty of Engineering, Soka University) for discussions on the context-dependent secondary structure formation. This work was supported in part by a Grant-in-Aid for Scientific Research and a Grant for the 21st Century COE Program from the Ministry of Education, Science, Sports, and Culture of Japan; a Grant for Scientific Research from the Japan Society for the Promotion of Science; and a Research Grant from the Ministry of Health, Labor and Welfare of Japan. This work also was supported in part by the National Project on Protein Structural and Functional Analyses from the MEXT of Japan.

References

Brandish, P.E., Chiu, C.S., Schneeweis, J., Brandon, N.J., Leech, C.L., Kornienko, O., Scolnick, E.M., Strulovici, B., and Zheng, W.J. 2006. A cell-based ultra-high-throughput screening assay for identifying inhibitors of D-amino acid oxidase. *J. Biomol. Screen.* **11:** 481–487.

Brünger, A.T., Adams, P.D., Clore, G.M., DeLano, W.L., Gros, P., Grosse-Kunstleve, R.W., Jiang, J.S., Kuszewski, J., Nilges, M., Pannu, N.S., et al. 1998. Crystallography and NMR system: A new software suite for macromolecular structure determination. *Acta Crystallogr. D Biol. Crystallogr.* **54:** 905–921.

Chumakov, I., Blumenfeld, M., Guerassimenko, O., Cavarec, L., Palicio, M., Abderrahim, H., Bougueleret, L., Barry, C., Tanaka, H., La Rosa, P., et al. 2002. Genetic and physiological data implicating the new human gene G72 and the gene for D-amino acid oxidase in schizophrenia. *Proc. Natl. Acad. Sci.* **99:** 13675–13680.

Collaborative Computational Project, Number 4. 1994. The CCP4 suite: Programs for protein crystallography. *Acta Crystallogr. D Biol. Crystallogr.* **50:** 760–763.

Fukui, K. and Miyake, Y. 1992. Molecular cloning and chromosomal localization of a human gene encoding D-amino-acid oxidase. *J. Biol. Chem.* **267:** 18631–18638.

Fukui, K., Watanabe, F., Shibata, T., and Miyake, Y. 1987. Molecular cloning and sequence analysis of cDNAs encoding pig kidney D-amino acid oxidase. *Biochemistry* **26:** 3612–3618.

Fukui, K., Momoi, K., Watanabe, F., and Miyake, Y. 1988. In vivo and in vitro expression of pig D-amino acid oxidase: In vitro system for the synthesis of a functional enzyme. *Biochemistry* **27:** 6693–6697.

Gouet, P., Robert, X., and Courcelle, E. 2003. ESPript/ENDscript: Extracting and rendering sequence and 3D information from atomic structures of proteins. *Nucleic Acids Res.* **31:** 3320–3323.

Holm, L. and Sander, C. 1993. Protein structure comparison by alignment of distance matrices. *J. Mol. Biol.* **233:** 123–138.

Krebs, H.A. 1935. Metabolism of amino-acids. III. Deamination of amino-acids. *Biochem. J.* **29:** 1620–1644.

Kuznetsov, I.B. and Rackovsky, S. 2003. On the properties and sequence context of structurally ambivalent fragments in proteins. *Protein Sci.* **12:** 2420–2433.

Mattevi, A., Vanoni, M.A., Todone, F., Rizzi, M., Teplyakov, A., Coda, A., Bolognesi, M., and Curti, B. 1996. Crystal structure of D-amino acid oxidase: A case of active site mirror-image convergent evolution with flavocytochrome b2. *Proc. Natl. Acad. Sci.* **93:** 7496–7501.

Michalopoulos, I., Torrance, G.M., Gilbert, D.R., and Westhead, D.R. 2004. TOPS: An enhanced database of protein structural topology. *Nucleic Acids Res.* **32:** D251–D254.

Miura, R., Setoyama, C., Nishina, Y., Shiga, K., Mizutani, H., Miyahara, I., and Hirotsu, K. 1997. Structural and mechanistic studies on D-amino acid oxidase-substrate complex: Implications of the crystal structure of enzyme-substrate analog complex. *J. Biochem.* **122:** 825–833.

Miyano, M., Fukui, K., Watanabe, F., Takahashi, S., Tada, M., Kanashiro, M., and Miyake, Y. 1991. Studies on Phe-228 and Leu-307 recombinant mutants of pig kidney D-amino acid oxidase: Expression, purification, and characterization. *J. Biochem.* **109:** 171–177.

Mizutani, H., Miyahara, I., Hirotsu, K., Nishina, Y., Shiga, K., Setoyama, C., and Miura, R. 1996. Three-dimensional structure of pig kidney D-amino acid oxidase at 3.0 Å resolution. *J. Biochem.* **120:** 14–17.

Mizutani, H., Miyahara, I., Hirotsu, K., Nishina, Y., Shiga, K., Setoyama, C., and Miura, R. 2000. Three-dimensional structure of the purple intermediate of porcine kidney D-amino acid oxidase. Optimization of the oxidative half-reaction through alignment of the product with reduced flavin. *J. Biochem.* **128:** 73–81.

Molla, G., Sacchi, S., Bernasconi, M., Pilone, M.S., Fukui, K., and Pollegioni, L. 2006. Characterization of human D-amino acid oxidase. *FEBS Lett.* **580:** 2358–2364.

Momoi, K., Fukui, K., Watanabe, F., and Miyake, Y. 1988. Molecular cloning and sequence analysis of cDNA encoding human kidney D-amino acid oxidase. *FEBS Lett.* **238:** 180–184.

Murshudov, G.N., Vagin, A.A., and Dodson, E.J. 1997. Refinement of macromolecular structures by the maximum-likelihood method. *Acta Crystallogr. D Biol. Crystallogr.* **53:** 240–255.

Nicholls, A., Sharp, K.A., and Honig, B. 1991. Protein folding and association: Insights from the interfacial and thermodynamic properties of hydrocarbons. *Proteins* **11:** 281–296.

Otwinowski, Z. and Minor, W. 1997. Processing of X-ray diffraction data collected in oscillation mode. *Methods Enzymol.* **276:** 307–326.

Park, H.K., Shishido, Y., Ichise-Shishido, S., Kawazoe, T., Ono, K., Iwana, S., Tomita, Y., Yorita, K., Sakai, T., and Fukui, K. 2006. Potential role for astroglial D-amino acid oxidase in extracellular D-serine metabolism and cytotoxicity. *J. Biochem.* **139:** 295–304.

Pilone, M.S. 2000. D-Amino acid oxidase: New findings. *Cell. Mol. Life Sci.* **57:** 1732–1747.

Pollegioni, L., Fukui, K., and Massey, V. 1994. Studies on the kinetic mechanism of pig kidney D-amino acid oxidase by site-directed mutagenesis of tyrosine 224 and tyrosine 228. *J. Biol. Chem.* **269:** 31666–31673.

Pollegioni, L., Diederichs, K., Molla, G., Umhau, S., Welte, W., Ghisla, S., and Pilone, M.S. 2002. Yeast D-amino acid oxidase: Structural basis of its catalytic properties. *J. Mol. Biol.* **324:** 535–546.

Raibekas, A.A., Fukui, K., and Massey, V. 2000. Design and properties of human D-amino acid oxidase with covalently attached flavin. *Proc. Natl. Acad. Sci.* **97:** 3089–3093.

Sawa, A. and Snyder, S.H. 2002. Schizophrenia: Diverse approaches to a complex disease. *Science* **296:** 692–695.

Setoyama, C., Miura, R., Nishina, Y., Shiga, K., Mizutani, H., Miyahara, I., and Hirotsu, K. 1996. Crystallization of expressed pig kidney D-amino acid oxidase and preliminary X-ray crystallographic characterization. *J. Biochem.* **119:** 1114–1117.

Setoyama, C., Nishina, Y., Tamaoki, H., Mizutani, H., Miyahara, I., Hirotsu, K., Shiga, K., and Miura, R. 2002. Effects of hydrogen bonds in association with flavin and substrate in flavoenzyme D-amino acid oxidase. The catalytic and structural roles of Gly313 and Thr317. *J. Biochem.* **131:** 59–69.

Thompson, J.D., Higgins, D.G., and Gibson, T.J. 1994. CLUSTAL W: Improving the sensitivity of progressive multiple sequence alignment through sequence weighting, position-specific gap penalties and weight matrix choice. *Nucleic Acids Res.* **22:** 4673–4680.

Todone, F., Vanoni, M.A., Mozzarelli, A., Bolognesi, M., Coda, A., Curti, B., and Mattevi, A. 1997. Active site plasticity in D-amino acid oxidase: A crystallographic analysis. *Biochemistry* **36:** 5853–5860.

Umhau, S., Pollegioni, L., Molla, G., Diederichs, K., Welte, W., Pilone, M.S., and Ghisla, S. 2000. The X-ray structure of D-amino acid oxidase at very high resolution identifies the chemical mechanism of flavin-dependent substrate dehydrogenation. *Proc. Natl. Acad. Sci.* **97:** 12463–12468.

Yagi, K., Nagatsu, T., and Ozawa, T. 1956. Inhibitory action of chlorpromazine on the oxidation of D-amino-acid in the diencephalon part of the brain. *Nature* **177:** 891–892.

Available online at www.sciencedirect.com
ScienceDirect
Biochemical and Biophysical Research Communications 350 (2006) 249–256
BBRC
www.elsevier.com/locate/ybbrc

The crystal structure of L-lactate oxidase from *Aerococcus viridans* at 2.1 Å resolution reveals the mechanism of strict substrate recognition

Yasufumi Umena [a,b], Kazuko Yorita [c], Takeshi Matsuoka [d], Akiko Kita [a,e], Kiyoshi Fukui [c], Yukio Morimoto [a,e,*]

[a] *Research Reactor Institute, Kyoto University, Kumatori, Osaka 590-0494, Japan*
[b] *Institute for Protein Research, Osaka University, Suita, Osaka 565-0871, Japan*
[c] *Institute for Enzyme Research, The University of Tokushima, Tokushima 770-8503, Japan*
[d] *Fine Chemicals and Diagnostics Division, Asahi Kasei Pharma, Shizuoka 410-2321, Japan*
[e] *RIKEN, Harima Institute at Spring-8, Kohto, Mikazuki, Hyogo 679-5148, Japan*

Received 31 August 2006
Available online 18 September 2006

Abstract

L-Lactate oxidase (LOX) from *Aerococcus viridans* is a member of the α-hydroxyacid-oxidase flavoenzyme family. We have determined the three-dimensional structure of LOX and revealed the mechanism of substrate recognition. The LOX monomer structure has a typical α_8/β_8 motif commonly found in other flavin family proteins. A related enzyme, glycolate oxidase, catalyzes the oxidation of glycolate rather than lactate. Comparison of the two enzyme structures highlights the importance of five residues around the FMN prosthetic group of LOX, which act synergistically to discriminate between the L/D configurations of lactate. X-ray crystallography of LOX gave a space group *I*422 of unit-cell parameters $a = b = 191.096$ Å, $c = 194.497$ Å and $\alpha = \beta = \gamma = 90°$ with four monomers per asymmetric unit. The four independent monomers display slight structural differences around the active site. Diffraction data were collected, under cryogenic conditions to 2.1 Å resolution at the synchrotron facilities in Japan.

Keywords: X-ray structure analysis; Lactate oxidase; Flavoprotein; Substrate recognition

The α-hydroxyacid oxidases are a group of flavoproteins that catalyze the flavin mononucleotide (FMN)-dependent oxidation of their respective substrates. The striking similarity in the catalytic properties of these oxidases, together with the presence of common structural motifs, suggests the enzymes constitute a distinct family. The known members of this family are lactate dehydrogenase (flavocytochrome b_2) [1], L-lactate monooxygenase [2], glycolate oxidase [3], L-mandelate dehydrogenase [4], and long-chain α-hydroxyacid oxidase [5]. Within the family, the crystal structures of glycolate oxidase [6], flavocytochrome b_2 [7], and the chimeric form of L-mandelate dehydrogenase [8] have been solved. Comparison of these structures reveal, similar protein folding patterns with each monomeric unit consisting of eight α-helices and eight β-strands in a typical α/β barrel arrangement, and with the FMN prosthetic group located at the C-terminal end of the β-strands.

L-Lactate oxidase (LOX) from *Aerococcus viridans* catalyzes the oxidation of L-lactate using molecular oxygen to generate pyruvate and H_2O_2 [9]. The flavoprotein displays a high level of substrate specificity and is able to differentiate between L-lactate and glycolate. The reaction mechanism and substrate specificity of α-hydroxyacid oxidases are based on the interaction of FMN with the respective substrate and adjacent amino acid residues in the active site. Therefore, determination of the three-dimensional structure of LOX is an important step in facilitating a more detailed mechanistic study of these flavoenzymes. Two Arg residues of LOX, Arg181 and Arg268, are conserved in all of the α-hydroxyacid

* Corresponding author. Fax: +81 724 51 2371.
E-mail address: morimoto@rri.kyoto-u.ac.jp (Y. Morimoto).

0006-291X/$ - see front matter © 2006 Elsevier Inc. All rights reserved.
doi:10.1016/j.bbrc.2006.09.025

oxidase family members. Based on the X-ray crystal structure of glycolate oxidase and flavocytochrome b_2, these two Arg residues are located in the vicinity of the FMN cofactor and are likely to form part of the substrate-binding site. We made a mutant of LOX in which Arg181 is replaced by Met (LOX–R181M) in order to determine the effect of removing the positive charge at this position [10]. Although the reactivity of LOX–R181M containing reduced FMN with oxygen was almost the same as wild-type enzyme, the efficiency of reduction of oxidized FMN by L-lactate was much lower [10]. These results demonstrate the participation of Arg181 in both the binding of substrate and in influencing the properties and reactivity of the active-site FMN. We previously reported the crystallization of wild-type enzyme, but the quality of the crystals was insufficient to solve the structure [11]. However, the crystallization of LOX–R181M with a small amount of additive reagent did yield high quality crystals for structural analysis. Here, we describe the crystal structure of wild-type LOX obtained by the same crystallization method used for the LOX–R181M mutant. Based on the determined structure, we discuss the mechanism of substrate recognition by LOX.

Experimental procedures

Purification of the L-lactate oxidase from Aerococcus viridans. Wild-type L-lactate oxidase (LOX) from *A. viridans* was purified to homogeneity as described previously [11]. Prior to crystallization the enzyme was passed through a Sephacryl S-200HR (Amersham Biosciences Corp., Piscataway, NJ) column and then concentrated to 20 mg ml^{-1} in 50 mM Tris–HCl, pH 8.0, using a Centricon YM-10 (Millipore, Billerica, MA). The protein concentration was determined using a molecular extinction coefficient at 456 nm of 11.0×10^3 M^{-1} cm^{-1} and a molecular weight of 40,865 [9].

Crystallization and data collection. Crystals of wild-type LOX suitable for data collection were obtained at 298 K using a sitting-drop vapor diffusion technique. The precise crystallization conditions were described in a previous report for the LOX–R181M mutant [12]. A 2.0-μl aliquot of wild-type protein solution at a concentration of 20 mg/ml in 50 mM Tris buffer (pH 8.0) was mixed with an equal volume of reservoir solution (18–20% (w/v) PEG 8000 and 50 mM Tris buffer at pH 8.0 and an additive solution of 2% (w/v) benzamidine–HCl). The crystals grew to full size ($0.05 \times 0.05 \times 0.1$ mm) after 2 weeks. Crystals were soaked in cryoprotectant (25% PEG 8000, 50 mM Tris–HCl buffer at pH 8.0 and 10% glycerol) for a few seconds and then flash-cooled to 100 K in a stream of dry nitrogen. The X-ray diffraction data were collected at beamlines BL44XU (DIP6040 imaging plate detector), BL41XU (MAR CCD detector), and BL38B1 (Rigaku Jupiter 210 CCD detector) at SPring-8, and BL12NW (ADSC Quantum 4 CCD detector) at the Photon Factory, Japan. The data were processed using HKL2000 and SCALEPACK [13]. The crystals of wild-type LOX belong to the tetragonal space group *I*422, with unit-cell parameters $a = b = 191.096$, $c = 194.497$ Å, which is identical to the R181M mutant [12]. Because the molecular mass of wild-type enzyme is 41 kDa, we assume there to be four monomers per asymmetric unit and thus 64 monomers in a unit cell, resulting in a Matthews coefficient (V_M) of 2.71 $Å^3$ Da^{-1} and a solvent content of 50.4%.

Structure determination and refinement. The structure was determined by the molecular replacement method using the program CNS [14]. Glycolate oxidase (Protein Data Bank entry 1GOX), which has 35.4% sequence identity to LOX at the amino acid level, was used as an initial search model. Self- and cross-rotation functions indicated the enzyme forms a tetramer. Thus, an initial search model was generated to a tetramer with non-crystallographic symmetry. All refinements were carried out using CNS and CCP4:REFMAC5 [15]. The structure was visualized and modified using XtalView [16] and Coot [17]. A refined model of wild-type LOX consisted of four molecules (Wild-A, wild-B, wild-C, and wild-D). The model geometry was analyzed with PROCHECK [18]. Data collection and refinement statistics are summarized in Table 1. The final coordinates and the structure factors have been deposited in the Protein Data Bank (entries 2DU2, rcsb025843).

Analysis for sequences and molecules. A multiple sequence alignment of wild-type LOX, glycolate oxidase (GOX), and L-lactate monooxygenase (LMO) was carried out in our previous report [9]. LSQKAB [19] in the program package CCP4 [20] was used for superposition of all the coordinates. The structures of wild-A, wild-B, wild-C, and wild-D could be superimposed between equivalent regions.

Table 1
Data collection and refinement statistics

Crystal data statistics	Wild type
X-ray source	SPring-8 BL38B1
Detector	Rigaku CCD Jupiter 210
Wavelength (Å)	1.00
Crystal-to-detector distance (mm)	205
Exposure time (s)	20
Data collection temperature (K)	100
No. of crystals per image	1/180
Space group	*I*422
Unit cell parameters	
$a = b$ (Å)	191.096
c (Å)	194.497
Resolution range (Å)	45.752-2.07
No. of total reflections	1,391,263
No. of unique reflections	108,566
$\langle I/\sigma(I)\rangle$	22.72
Completeness (%)	100.0(100.0)[a]
R_{merge} (%)	14.2(43.6)[a]
Redundancy	12.8(10.5)[a]
No. of molecules per asymmetric unit	4
V_M ($Å^3$ Da^{-1})	2.71
Resolution range (Å)	46.0–2.07
σ Cutoff (F)	0.0
R_{cryst}[b] (%)	16.23
R_{free}[c] (%)	19.98
No. of atoms	
No. of protein atoms	11,564
No. of prosthetic atoms	124
No. of water molecules	1110
Average *B*-factor	
All	19.472
Proteins	18.986
Prosthetic group	13.092
Water molecules	25.302
rmsd for bonds (Å)	0.018
rmsd for angles (°)	1.782
Ramachandran plot (%)	
Most favored	88.7
Additional allowed	10.3
Generously allowed	0.5
Disallowed	0.5

[a] Values in parentheses are for the highest-resolution shell.
[b] R_{cryst} was calculated from the working set (95% of the data).
[c] R_{free} was calculated from the test set (5% of the data).

Results

Overall structure of the L-lactate oxidase from A. viridans

Wild-type LOX crystals belong to space group *I*422 with 64 molecules in a unit cell and four molecules per asymmetric unit (Fig. 1a). The overall fold (Fig. 1b) of the LOX monomer was a $(\beta/\alpha)_8$-barrel first observed in a triose-phosphate isomerase [21]. A schematic drawing of the structure is given in Fig. 2. The helices and strands corresponding to the canonical α/β barrel have been numbered α1 (residues 105–116), α2 (129–136), α3 (151–164), α4 (224–233), α5 (246–255), α6 (276–287), α7 (302–311), α8 (331–352), β1 (89–91), β2 (118–122), β3 (144–145), β4 (169–172), β5 (238–241), β6 (259–262), β7 (293–295), and β8 (315–319). The N-terminal region has some helices and strands; αA (residues 22–32), αB (35–42), αC (49–60), βB (78–80), and βC (83–85). αG (357–362) is located in the C-terminal region. βB and βC are located at the bottom of the barrel where they form an anti-parallel β-sheet lid structure. Three helices, αC′ (residues 97–100), αD (182–187), and αF (320–328), are inserted into the (β/α) repetition (β1–α1, β4–α4, and β8–α8) in the barrel. The αD helix connects β4 to α4 with a long flexible chain (residues 188–223) and this region is located at the top of the barrel. These secondary structures are common to the four monomers of LOX. The r.m.s. deviations of the main chain among the four monomers, excluding the terminal regions (1–21, 363–374) and flexible regions (173–225, 263–275), were 0.701 Å (wild-A/B; maximum), 0.621 Å (wild-A/C), 0.635 Å (wild-A/D), 0.451 Å (wild-B/C), 0.513 Å (wild-B/D), and 0.421 Å (wild-C/D; minimum). These calculations suggest that wild-A differs slightly amongst the other three monomers.

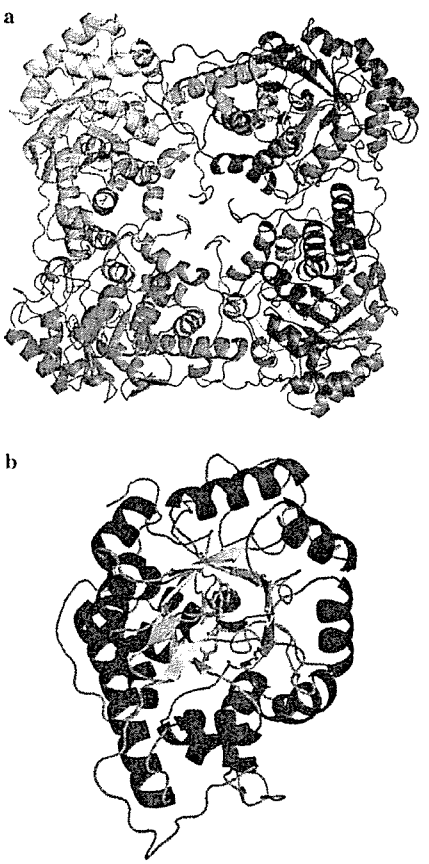

Fig. 1. Crystal structure of the L-lactate oxidase (LOX) from *Aerococcus viridans* at 2.1 Å resolution. (a) Tetramer form of the LOX. The blue to red color corresponds to the N- and C-terminal region within the four monomers. (b) One subunit of the tetramer (wild-A molecule). Red is α-helices, yellow is β-strand, and light blue is the FMN group. (For interpretation of the references to color in this figure legend, the reader is referred to the web version of this paper.)

Quarternary structure of the enzyme

Molecular exclusion chromatography using Sephadex G-100 initially suggested that wild-type LOX exists as a tetramer in 50 mM potassium phosphate buffer, pH 7.0, in the presence of 0.2 M potassium chloride [22]. Furthermore, our LOX crystals possess four monomers per asymmetric unit, suggesting that the enzyme is catalytically active as a tetramer in solution. Wild-type LOX forms a tetramer with a non-crystallographic fourfold symmetry in the center of the tetramer (Fig. 1a). Four C-terminal regions and αC helices are gathered into the center of the tetramer. The barrel of the monomer is inclined by about 45° to the non-crystallographic fourfold axis. The N-terminal flexible region and αA, αB helices are located at one side ('back side') of the tetramer, where they form a depression. Glycolate oxidase (GLO) also crystallizes with space group *I*422(6), but in this case a non-crystallographic unit is occupied by just one monomer. The crystal packing of GLO yields an octamer with a strict crystallographic symmetry. Two tetramers of GLO are related by a twofold axis of symmetry so that the depression area of each tetramer is covered by the apposing tetramer.

Comparison of the amino acid sequence and Tertiary structure of LOX and GLO

The three related enzymes LOX, GLO, and lactate monooxygenase are composed of a similar number of amino acids (374, 369, and 393, respectively). Amino acid residues that form the binding pocket for the FMN cofactor are well-conserved between the three enzymes. The conserved residues are located at the top of the barrel, at least for LOX and GLO which have a determined structure. GLO has no chain in this region of the protein (189–197, GLO). The superposition of LOX and GLO shows a slight discrepancy in the barrel, the r.m.s. deviation between the two barrels being 1.40 Å.

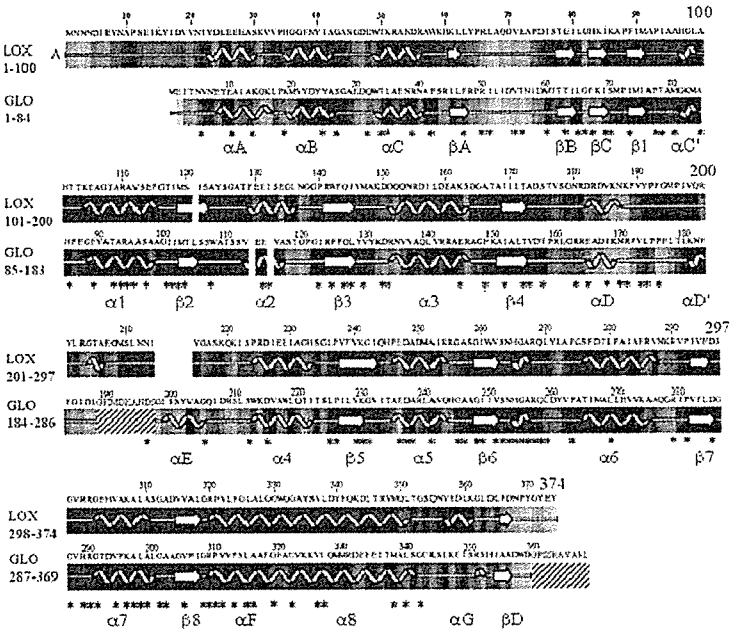

Fig. 2. Schematic drawings and comparison of LOX and GLO. Secondary structures were drawn using the program PROCHECK. The red shadowed portions in the GLO are not determined in the three-dimensional structure. Asterisks indicate identical residues found in both LOX and GLO. (For interpretation of the references to colour in this figure legend, the reader is referred to the web version of this paper.)

Comparison of the temperature factors among LOX and GLO

Fig. 3 shows the temperature factors for each monomer of LOX. Each monomer of the LOX tetramer has a common distribution of temperature factors, except for some flexible regions (1–10 and 190–210). The temperature factors of the central region of the tetramer are relatively low compared with the molecular surface of the tetramer. In each monomer, segments of the sequence (residues 46–62, 240–245, 276–281, and 296–311) were regarded as internal regions of the tetramer. The average value of temperature factors for such amino acid residues was 10.066, compared to a total average value of 17.344. This feature is also evident for the respective monomers. By contrast, however, there is no such distribution of temperature factors at equivalent regions of the GLO monomer (i.e., 20.684 for residues 30–46, 229–234, 265–270, and 286–301, and 27.190 for the overall average).

Comparison of the residues around the active site

Based on the r.m.s. deviations, no significant structural differences were evident between the four monomers that make up the tetramer. Thus, each monomer does not undergo independent movement with respect to the tetramer. The superimposed structures of LOX and GLO (Fig. 4) display conserved regions surrounding amino acids, Y40, R181, and H265 (numbering corresponds to LOX). The catalytic mechanism of LOX was discussed in our previous report [9]. The following amino acids play critical roles in the reaction mechanism of GLO: Y24, Y129, R164, K230, H254, R257, R289, and R309. Our structure of LOX shows that these residues are well-conserved: Y40, Y146, R181, K241, H265, R268, R300, and R320.

Discussion

Molecular structure of the L-lactate oxidase

The tertiary structure of wild-type LOX has a typical β8/α8 barrel structure with some extra helices and strands. The quaternary structure of the enzyme is a tetramer in which each of the four monomers adopts an almost identical structure. Flavin enzymes may adopt a typical β8/α8 barrel structure, such as flavocytochrome *b*2 flavin domain and GLO. Although GLO is frequently used as a model for the analysis of LOX, the complete structure of LOX is slightly twisted around the axis of the barrel when each FMN group is fitted. The lid region may act to stabilize the enzyme when it selects lactate as substrate rather than glycolate. The K_m value of the LOX mutant R181M is larger than that of the wild-type enzyme. The single amino acid substitution R181M affects amino acid residues near the FMN group, but does not interfere with the formation of tetramer. Consequently, the larger K_m value of the mutant is a result of an alteration in the region of the active site that specifically interacts with the substrate, without there being major structural changes to the surrounding amino acid residues.

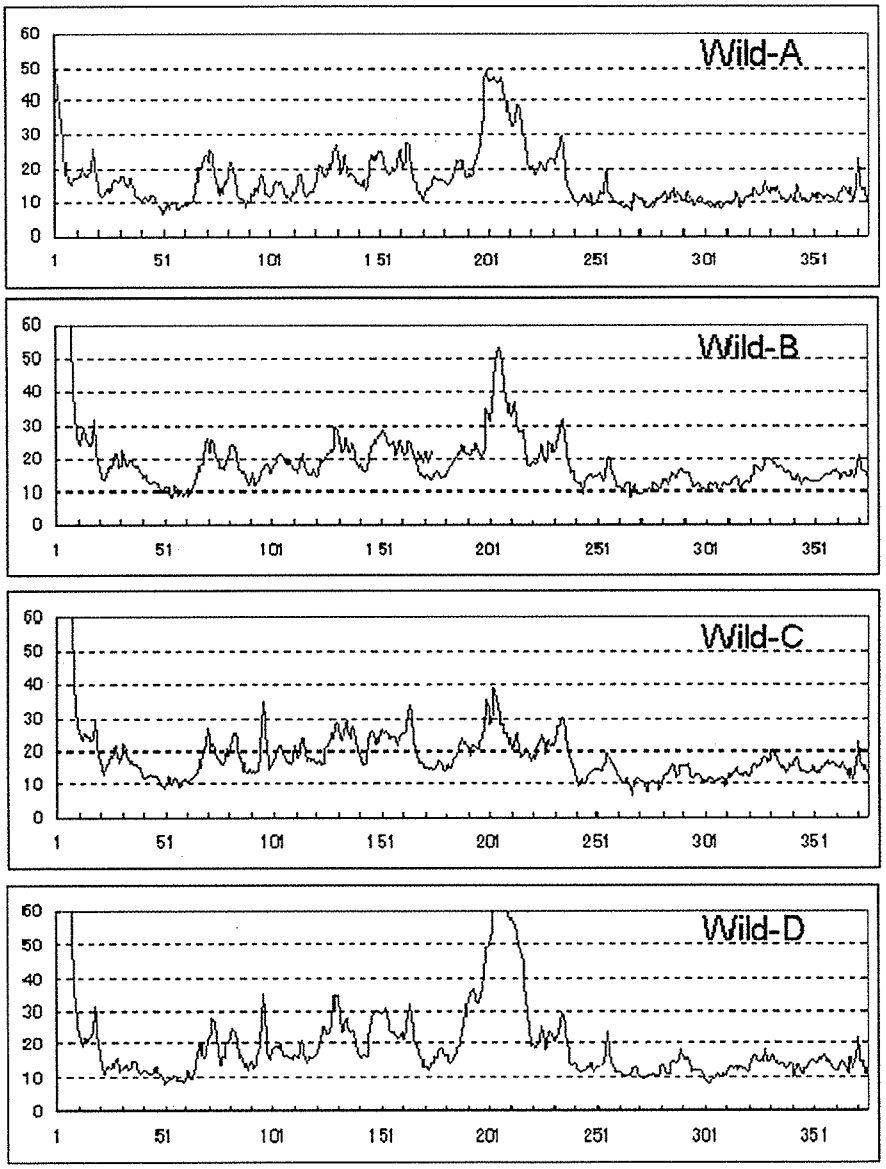

Fig. 3. Temperature factors for each subunit of the LOX. Plots are only for Cα atoms.

Substrate recognition of L-lactate oxidase

The LOX enzyme catalyzes the conversion of L-lactate to pyruvate mediated by the FMN group. The Arg268, His265, and Tyr40 are critical for the mechanism of catalysis as shown in the schematic representation of the reaction in Fig. 5. The tetramer is associated with 1110 water molecules, 904 of which are located inside the enzyme. Interestingly, two water molecules were found in the active site cavity of each monomer: 5647 and 5694 for wild-A; 5139 and 5125 wild-B; 5455 and 5040 wild-C; 5585 and 5447 wild-D. The water molecules 5694, 5125, 5040, and 5447 are close to the three residues, Y40, R268, and R181, respectively. Water molecules 5647, 5139, 5455, and 5040 are surrounded by residues Y215, H265, and R181, respectively (Fig. 6a). Structural analysis of flavocytochrome *b*2 and the pyruvate complex suggests the pyruvate product is located close to the FMN group. Superimposed structures of pyruvate-bound flavocytochrome *b*2 and LOX show that the two water molecules in the active site of LOX are located in an equivalent position to pyruvate in flavocytochrome *b*2. Therefore, in the absence of L-lactate, the two water molecules occupy the active site of LOX. The reaction mechanism of GLO [6] involves the FMN cofactor accepting the electron from glycolate. Although lactate differs from glycolate only by the presence of an additional methyl group, the two compounds are markedly different in terms of dipole moment and occupancy of space around the FMN group. LOX contains sufficient space to house lactate but not glycolate. The structure of the active site of LOX includes space for L-lactate on the FMN plane

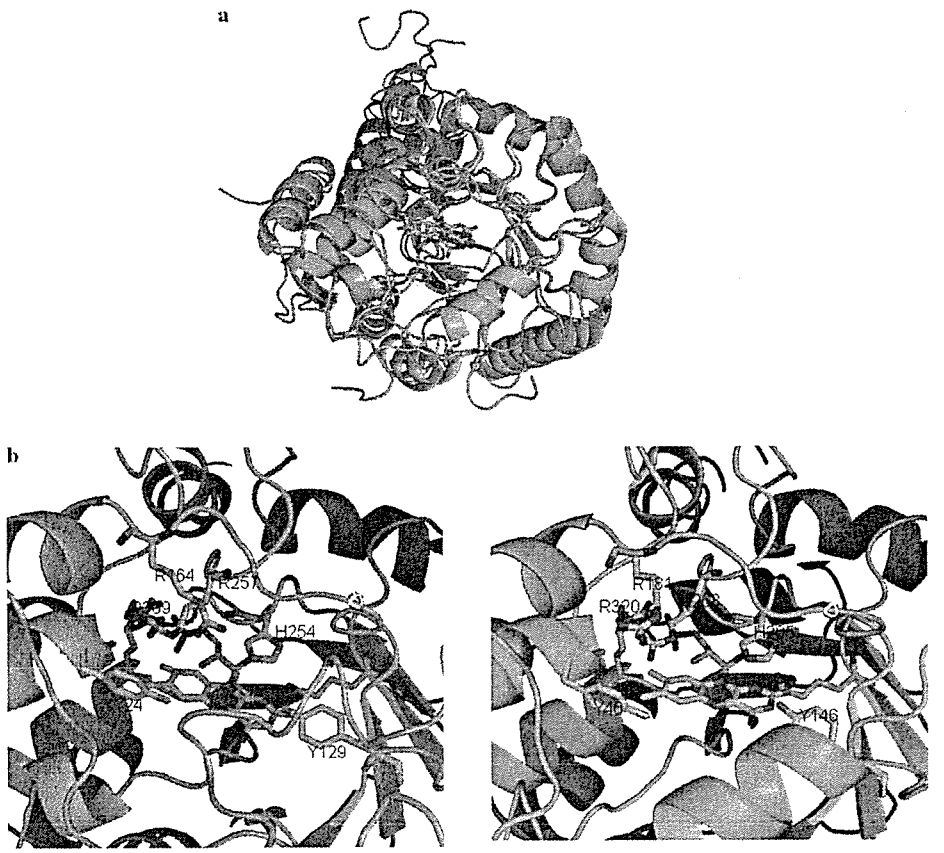

Fig. 4. Superimposed structures of LOX and GLO. Light blue is LOX and green GLO. (a) The LOX wild-A subunit and GLO, (b) active site with FMN, and Tyr, Arg, and His residues: left, GLO; right, LOX. Residue numbers correspond to the respective amino acid sequence.

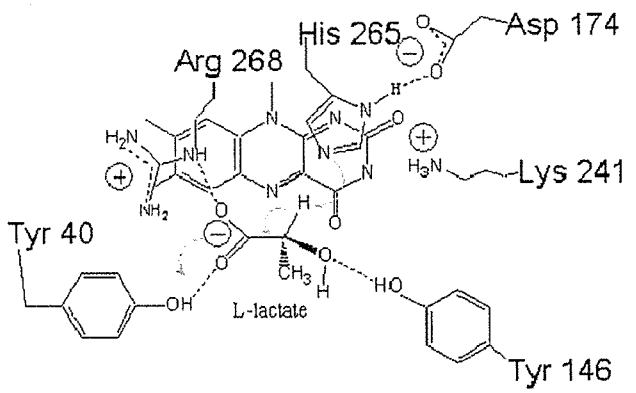

Fig. 5. Schematic representation of the reaction mechanism on the FMN by the residues Y40, Y146, D174, H265, and R268.

surrounding residues at least Y40, Y146, and H265. The geometrical arrangement of these residues provides compelling evidence for the location of the L-lactate substrate. Although the Y215 and L211 are located in the flexible region among four monomers, at least in the wild-A the two residues may perform a plausible combination to recognize a substrate (Fig. 6a). Three OH-groups of the Tyr residues are located on the same plane supported from both sides by H265 and L211. When H265 is on the right side of the plane, L211 should be on the left. The methyl moiety of L-lactate, being hydrophobic, is fixed by L211 on the left-hand side of the plane when lactate is located on the FMN (Fig. 6b), thereby providing specific substrate recognition. When the carboxyl moiety of L-lactate is orientated close to Y40 (top of Fig. 6b) with the hydroxyl oxygen facing toward H265, the position of the methyl group is dictated by L211. Thus, the three Tyr residues (Y40, Y146, and Y215) together with H265 and L211 of LOX function synergistically to determine the chirality of the substrate. GLO displays no such D/L specificity for substrate even though the enzyme has a similar configuration of Tyr and His residues (Y24, Y129, and H254) in the active site.

The oxidative decarboxylation of pyruvate to form acetyl-CoA is the link between glycolysis and the tricarboxylic acid cycle. In bacteria, L-lactate oxidase is also a critical intermediate in primary metabolism. Here we have determined the structure of LOX and proposed the mechanism of substrate specificity for D/L-lactate. To fully characterize the catalytic mechanism of LOX at atomic resolution it will be necessary to determine the three-dimensional structures of LOX with L-lactate or pyruvate.

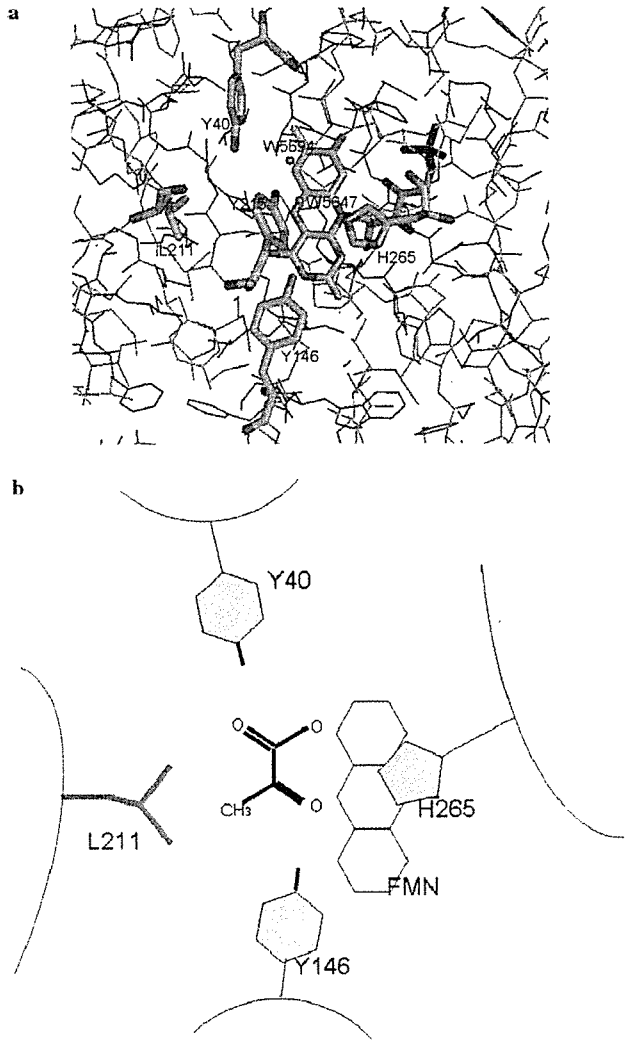

Fig. 6. Active site of LOX and some important residues for strict substrate recognition. (a) Two water molecules (W5647 and W5694) in the cavity composed of FMN, Y40, Y146, Y215, L211, and H265, (b) schematic representation of molecular recognition between LOX and L-lactate. Substrate is recognized by the following residues: orientation of L-lactate is determined by Y40, Y146, and Y215; right and left positioning is fixed by H265 and L211.

Acknowledgments

We thank Prof. T. Tsukihara at Osaka University for useful discussion of this work. This research was partly supported by a Grant-in-aid for the National Project on Protein Structural and Function Analysis (to Y.M.) and the Project Nos. 17053011 and 13680749 (to Y.M.) from the Ministry of Education, Culture, Sports, Science, and Technology of Japan, for which the authors are greatly appreciative. This research was conducted with prior approval of SPring-8, the Institute for Protein Research (Proposal 2004A0652-NL1-np-P3k and 2004B0598-NL1-np for BL38B1, BL41XU, C05A44XU-7226-N for BL44XU), the Photon Factory Advisory Committee, and the National Laboratory for High Energy Physics, Japan (Proposal 2004G348 for BLNW12, BL6A).

References

[1] Y. Lindqvist, C.I. Branden, F.S. Mathews, F. Lederer, Spinach glycolate oxidase and yeast flavocytochrome b_2 are structurally homologous and evolutionarily related enzymes with distinctly different function and flavin mononucleotide binding, J. Biol. Chem. 266 (5) (1991) 3198–3207.

[2] U. Ermler, S. Ghisla, V. Massey, G.E. Schulz, Structural, spectroscopic and catalytic activity studies on glutathione reductase reconstituted with FAD analogues, Eur. J. Biochem. 199 (1) (1991) 133–138.

[3] Y. Lindqvist, C.I. Branden, The active site of spinach glycolate oxidase, J. Biol. Chem. 264 (6) (1989) 3624–3628.

[4] B. Mitra, J.A. Gerlt, P.C. Babbitt, C.W. Koo, G.L. Kenyon, D. Joseph, G.A. Petsko, A novel structural basis for membrane association of a protein: construction of a chimeric soluble mutant of (*S*)-mandelate dehydrogenase from *Pseudomonas putida*, Biochemistry 32 (48) (1993) 12959–12967.

[5] K.H. Diep Lê, F. Lederer, Amino acid sequence of long chain alpha-hydroxy acid oxidase from rat kidney, a member of the family of FMN-dependent alpha-hydroxy acid-oxidizing enzymes, J. Biol. Chem. 266 (31) (1991) 20877–20881.

[6] Y. Lindqvist, Refined structure of spinach glycolate oxidase at 2 Å resolution, J. Mol. Biol. 209 (1) (1989) 151–166.

[7] Z.X. Xia, F.S. Mathews, Molecular structure of flavocytochrome b_2 at 2.4 Å resolution, J. Mol. Biol. 212 (4) (1990) 837–863.

[8] N. Sukumar, Y. Xu, D.L. Gatti, B. Mitra, F.S. Mathews, Structure of an active soluble mutant of the membrane-associated (*S*)-mandelate dehydrogenase, Biochemistry 40 (33) (2001) 9870–9878.

[9] K. Maeda-Yorita, K. Aki, H. Sagai, H. Misaki, V. Massey, L-Lactate oxidase and L-lactate monooxygenase: mechanistic variations on a common structural theme, Biochimie 77 (1995) 631–642.

[10] K. Yorita, T. Matsuoka, H. Misaki, V. Massey, Interaction of two arginine residues in lactate oxidase with the enzyme flavin: conversion of FMN to 8-formyl-FMN, Proc. Natl Acad. Sci. USA 97 (24) (2000) 13039–13044.

[11] Y. Morimoto, K. Yorita, K. Aki, H. Misaki, V. Massey, L-Lactate oxidase from *Aerococcus viridans* crystallized as an octamer. Preliminary X-ray studies, Biochimie 80 (4) (1998) 309–312.

[12] Y. Umena, K. Yorita, T. Matsuoka, M. Abe, A. Kita, K. Fukui, T. Tsukihara, Y. Morimoto, Crystallization and preliminary X-ray diffraction study of L-lactate oxidase (LOX), R181M mutant, from *Aerococcus viridans*, Acta Cryst. F61 (2005) 439–441.

[13] Z. Otwinowski, W. Minor, Processing of X-ray diffraction data collected in oscillation mode, in Methods in Enzymology, Macromolecular Crystallography, part A: 276 (1997) 307–326.

[14] A.T. Brünger, P.D. Adams, G. Marius Clore, W.L. DeLano, P. Gros, R.W. Grosse-Kunstleve, J.S. Jiang, J. Kuszewski, M. Nilges, N.S. Pannu, R.J. Read, L.M. Rice, T. Simonson, G.L. Warren, Crystallography and NMR system: a new software suite for macromolecular structure determination, Acta Cryst. D54 (1998) 905–921.

[15] G.N. Murshudov, A.A. Vagin, E.J. Dodson, Refinement of macromolecular structures by the maximum-likelihood method, Acta Cryst. D53 (1997) 240–255.

[16] D.E. McRee, Practical Protein Crystallography, Academic Press, New York, 1993.

[17] P. Emsley, K. Cowtan, Coot: model-building tools for molecular graphics, Acta Cryst. D60 (2004) 2126–2132.

[18] R.A. Laskowski, M.W. MacArthur, D.S. Moss, J.M. Thornton, PROCHECK: a program to check the stereochemical quality of protein structures, J. App. Cryst. 26 (1993) 283.

[19] W. Kabsch, A solution for the best rotation to relate two sets of vectors, Acta Cryst. A32 (1976) 922–923.
[20] Collaborative computational project, Number 4The CCP4 suite: programs for protein crystallography, Acta Cryst. D50 (1994) 760–763.
[21] D.W. Banner, A.C. Bloomer, G.A. Petsko, D.C. Phillips, C.I. Pogson, I.A. Wilson, P.H. Corran, A.J. Furth, J.D. Milman, R.E. Offord, J.D. Priddle, S.G. Waley, Structure of chicken muscle triose phosphate isomerase determined crystallographically at 2.5 Å resolution using amino acid sequence data, Nature 255 (1975) 609–614.
[22] J.D. Duncan, J.O. Wallis, M.R. Azari, Purification and properties of *Aerococcus viridans* lactate oxidase, Biochem. Biophys. Res. Commun. 164 (2) (1989) 916–926.

FEBS Letters 580 (2006) 2358–2364

Characterization of human D-amino acid oxidase

Gianluca Molla[a], Silvia Sacchi[a], Mariagrazia Bernasconi[a], Mirella S. Pilone[a], Kiyoshi Fukui[b], Loredano Pollegioni[a,*]

[a] *Department of Biotechnology and Molecular Sciences, University of Insubria, Varese, Italy*
[b] *The University of Tokushima, The Institute for Enzyme Research, Tokushima, Japan*

Received 20 February 2006; revised 9 March 2006; accepted 12 March 2006

Available online 24 March 2006

Edited by Stuart Fergusan

Abstract **D-Amino acid oxidase (DAAO) has been proposed to be involved in the oxidation of D-serine, an allosteric activator of the NMDA-type glutamate receptor in the brain, and to be associated with the onset of schizophrenia. The recombinant human DAAO was expressed in *Escherichia coli* and was isolated as an active homodimeric flavoenzyme. It shows the properties of the dehydrogenase-oxidase class of flavoproteins, possesses a low kinetic efficiency, and follows a ternary complex (sequential) kinetic mechanism. In contrast to the other known DAAOs, the human enzyme is a stable homodimer even in the apoprotein form and weakly binds the cofactor in the free form.**

Keywords: Schizophrenia; Flavoprotein; Neurotransmission

1. Introduction

D-Amino acid oxidase (EC 1.4.3.3, DAAO) was one of the first flavoproteins to be discovered in the mid-thirties of the last century [1] and has played a prominent role in the development of present concepts in mechanistic flavin enzymology. It is a peroxisomal enzyme that catalyzes the deamination of D-amino acids to their imino acid counterparts with concomitant reduction of FAD. The reduced flavin is subsequently reoxidized by molecular oxygen generating H_2O_2, and the imino acid is released into solvent, where it spontaneously hydrolyzes to the corresponding α-keto acid and ammonia.

In yeast, DAAO is involved in the metabolic utilization of D-amino acids; in mammals its function is still uncertain. This question remained largely unanswered until recently when it was demonstrated that, in brain, the concentration of DAAO is reciprocal to that of D-serine, a neuromodulator that binds the glycine modulatory site on the NMDA receptor and that is needed for glutamate to activate the receptor [2]. The evidence that by exogenous application of DAAO D-serine degradation attenuates the NMDA receptor-mediated neurotransmission suggested that, in brain, this flavoenzyme degrades D-serine to regulate NMDA neurotransmission [3].

Schizophrenia affects nearly 1% of the world's population and accounts for about 2.5% of health-care costs. In the past few years several genes linked to schizophrenia susceptibility have been discovered. The most intriguing discovery has been a new human gene, G72 on chromosome 13q34. Yeast two-hybrid experiments with pLG72 identified DAAO on 12q24 as an interacting partner and functional measurements showed that pLG72 behaves as an in vitro activator of DAAO [4]. In this way, pLG72 could regulate glutamatergic signaling through the NMDA receptor pathway. Recombinant pLG72 was recently over-expressed in *Escherichia coli* and its main properties have been reported [5].

With the ambitious goal of contributing to the understanding of the correlation between modulation of the enzymatic activity in this flavoprotein and its possible role in neurotransmission and schizophrenia susceptibility, we investigated the main properties of human DAAO (hDAAO). The functional and structural properties of the enzyme from pig kidney (pkDAAO, 84% sequence identity to hDAAO) and from the yeast *Rhodotorula gracilis* (RgDAAO) have been extensively studied [6–8]. Although the cDNA encoding hDAAO was isolated in 1988 [9], only little has been undertaken to biochemically characterize the human enzyme, mainly because it was difficult to express in a heterologous system such as *E. coli*. Previous work focused on the artificial flavinylation of the apoprotein form of G218C mutant of hDAAO with 8-methylsulfonyl FAD [10]. Although this work reached the goal of obtaining a flavinylated enzyme, the wild-type hDAAO has not yet been functionally characterized in detail.

2. Materials and methods

2.1. Protein purification

The recombinant hDAAO is expressed in *E. coli* BL21(DE3) cells using the pET11b expression vector. The best yield (6.7 mg of hDAAO/liter of fermentation broth) was obtained by growing the cells overnight at 37 °C following induction with 0.6 mM IPTG during the exponential phase of growth. hDAAO is purified using a procedure modified from [10], consisting of ammonium sulfate precipitation at 35% saturation, followed by dialysis of the pellet, and anionic exchange chromatography on DEAE Sepharose FF at pH 8.0. Following this procedure, 4.2 mg of hDAAO/liter of fermentation broth with a 85% purity (estimated by SDS–PAGE) was purified, with an overall purification yield of 60%. For structural experiments, this latter enzyme sample was further purified by gel-permeation chromatography on a HiLoad Superdex 200 column (Amersham Biosciences). The final enzyme preparation was stored at −20 °C in 20 mM Tris–HCl, pH 8.0, 100 mM NaCl, 5% glycerol, 5 mM 2-mercaptoethanol, 40 μM FAD.

*Corresponding author. Fax: +39 0332 421500.
E-mail address: loredano.pollegioni@uninsubria.it (L. Pollegioni).

Abbreviations: DAAO, D-amino acid oxidase; hDAAO, D-amino acid oxidase from human; pkDAAO, D-amino acid oxidase from pig kidney; RgDAAO, D-amino acid oxidase from *Rhodotorula gracilis*; D-AA; D-amino acid; IA, imino acid

0014-5793/$32.00
doi:10.1016/j.febslet.2006.03.045

2.2. Determination of the oligomeric state

The oligomeric state of hDAAO was determined by gel-permeation chromatography on a Superdex 200 (Amersham Biosciences) column using 20 mM Tris–HCl, pH 8.5, 150 mM NaCl, 5% glycerol, 5 mM 2-mercaptoethanol, and 40 μM FAD as elution buffer.

2.3. Spectroscopy

Absorbance data were recorded at 15 °C in 20 mM Tris–HCl, 5% glycerol, and 5 mM 2-mercaptoethanol, pH 8.0, except where stated otherwise. Dissociation constants for ligands were measured spectrophotometrically by adding small volumes (1–10 μl) of concentrated stock solutions to samples containing 1 ml of ≈10 μM enzyme, at 15 °C, and have been calculated from the change in absorbance at 495 and 550 nm for benzoate and anthranilate, respectively. Because of the weak binding of the coenzyme to the apoprotein moiety, the reactions also reflect the shift of the APO + FAD ↔ HOLO equilibrium towards the final product upon binding of the ligand. Anaerobic samples were prepared in anaerobic cuvettes by applying 10 cycles of evacuation and then flushing with oxygen-free argon. Photoreduction experiments were carried out at 4 °C using an anaerobic cuvette containing ≈8 μM enzyme, 1 mM EDTA [11,12]. The solution was photoreduced with a 250 W lamp and the progress of the reaction was followed spectrophotometrically. The redox potential for the $E\text{-}FAD_{ox}/E\text{-}FAD_{red}$ couple of hDAAO was determined by the method of dye equilibration described by Massey [13]. The enzyme solution in 20 mM Tris–HCl, pH 8.0, 5% glycerol, was mixed in an anaerobic cuvette with 0.2 mM xanthine, 5 μM benzyl viologen as mediator, and 5–8 μM of the appropriate dye [13,14]. The solution was purged of oxygen, and the reaction was initiated by adding 10 nM xanthine oxidase. The course of the reaction was followed by recording the spectral course at 15 °C. Data were analyzed as described in [14,15].

All fluorescence measurements were performed at 15 °C and at 0.1 mg/ml protein concentration. The binding constant for the coenzyme was determined by titrating 1 μM apoprotein with increasing amounts of FAD and by monitoring the reconstitution following the quenching of the protein fluorescence at 340 nm [16]. Circular dichroism (CD) spectra were recorded on a Jasco J-810 spectropolarimeter and analyzed by means of Jasco software. For measurements above 250 nm, the cell path was 1 cm and for measurements in the 190–250 nm region was 0.1 cm.

2.4. Kinetic measurements

The apparent kinetic parameters on different amino acids as substrate were determined in 100 mM sodium pyrophosphate buffer, pH 8.5, containing 40 μM FAD, at 25 °C and air saturation, measuring the oxygen consumption with a Hansatech oxygen electrode [11].

The rapid reaction measurements and the turnover experiments were performed in 50 mM sodium pyrophosphate buffer, pH 8.3, containing 1% glycerol, at 25 °C in a stopped-flow BioLogic SFM-300 spectrophotometer equipped with a J&M diode array detector [17]. Enzyme monitored turnover data were analyzed according to the method described by [18]. For reductive and oxidative half-reaction experiments, the stopped-flow instrument was made anaerobic by overnight equilibration with a sodium dithionite solution and then was rinsed with argon-equilibrated buffer. Reaction rates were calculated by extracting traces at individual wavelengths (455 and 530 nm) and fitting them to a sum of exponentials equation using the program Biokine32 (BioLogic). The program Specfit/32 (Spectrum Software Ass., USA) was employed to simulate the experimental time courses.

3. Results

3.1. Spectral properties of purified hDAAO

The recombinant protein is isolated as a holoenzyme showing the typical absorbance spectrum of the FAD-containing flavoenzymes: absorbance maxima at 454, 372, and 278 nm and a ratio of the near-UV (~280 nm) and of the main visible band (455 nm) of ~10.6 (see Table 1 and Fig. 1). The absorption spectrum of oxidized hDAAO shows a marked dependence on pH: at high pH values (⩾ 10) a bathochromic shift is observed for the near-UV band at ~370 nm. This is consis-

Table 1
Comparison of the main properties of DAAO from different sources

	hDAAO	pkDAAO[a]	RgDAAO[a]
Spectral properties			
$\lambda_{455\,nm}$ ($mM^{-1}\,cm^{-1}$)	12.2	11.3	12.6
pK_a N(3)-H FAD	10.3 ± 0.2	9.4	10.6
Semiquinone formed (%)			
pH 8.0	<5[b]	90	94[c]
pH 8.3	77[b]		
E_m (mV), pH 8.0			
Free form	−100 ± 11	−138	−116
Benzoate complex	−134 ± 8	−185	−116
Structural and binding properties			
Length (amino acids)	347	347	368
Oligomeric state			
Holoenzyme	Dimeric	Isodesmic self-association	Dimeric
Apoprotein	Dimeric	Monomeric	Monomeric
FAD binding, K_d (M)			
Free form	$8 \pm 2 \times 10^{-6}$	2×10^{-7}	2×10^{-8}
Benzoate complex	$3 \pm 1 \times 10^{-7}$		
Benzoate binding, K_d (μM)	7 ± 2	2.0	245
Sulfite binding, K_d (μM)	64 ± 9	3500	110

[a]Refs. [6,19].
[b]The value depends on the experimental conditions used.
[c]Kinetically stabilized.

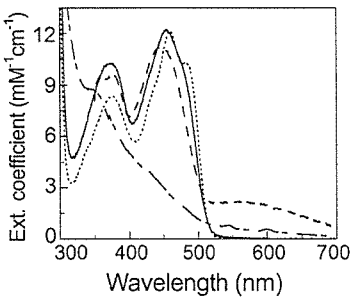

Fig. 1. Absorbance spectrum of hDAAO in the free (—), benzoate-complex (···) and anthranilate-complex (---) oxidized form and in the reduced form (——). The spectra of the hDAAO–ligand complexes have been obtained starting from the stock enzyme solution (containing 40 μM free FAD, see Section 2) diluted 45-fold in plain buffer (see below) and following the addition of 0.075 mM benzoate and 2.65 mM anthranilate to ~10 μM oxidized enzyme (the spectra were recorded 15 min after ligand addition). The spectrum of the reduced hDAAO was measured 90 min after the anaerobic addition of 5 mM D-alanine. *Conditions.* 20 mM Tris–HCl, pH 8.0, 5% glycerol, 5 mM 2-mercaptoethanol at 15 °C.

tent with N(3)-H of bound FAD not being ionized at physiological pH. The observed pK_a value (10.30 ± 0.15) is higher than that of free FAD and pkDAAO (~10.0 and 9.4, respectively). The enzyme tightly binds benzoate, a classical DAAO inhibitor, resulting in the typical perturbation of the flavin spectrum reported in Fig. 1. A K_d of 7 ± 2 μM at pH 8.0 was estimated. The enzyme also binds anthranilate (K_d = 40 ± 10 μM), yielding the typical "charge-transfer" absorption band centered around 580 nm (Fig. 1). When a sulfite covalent adduct to the N(5) flavin position is formed, the visible spectrum of the enzyme is bleached: a K_d of 64 ± 9 μM was estimated. This reaction is prevented by the addition of 0.1 mM benzoate.

The purified hDAAO is catalytically active as demonstrated by the conversion of the oxidized form of the flavin cofactor to the reduced state following the addition of D-alanine under anaerobic conditions (Fig. 1). Upon anaerobic photoreduction, the amount of the anionic semiquinone form of the flavin cofactor produced by hDAAO is largely dependent on the experimental conditions used. At pH 8.0 and in the presence of 20 mM Tris–HCl buffer, an amount of <5% of the semiquinone form was produced, while at pH 8.3 and in the presence of 50 mM bicine buffer, an amount of ~77% of the one-electron reduced form was formed. A large part of the semiquinone flavin form produced under the latter conditions is kinetically stabilized: following an overnight incubation, a 30% residual semiquinone form was observed (Table 1).

The midpoint redox potential of hDAAO was determined at pH 8.0 by the equilibration method [13] using indigodisulfonate as reference dye. For the two-electron transfer potential an $E_m \sim -100 \pm 11$ mV was estimated (Table 1). The addition of 1 mM benzoate caused a 34-mV negative shift of the midpoint redox potential.

3.2. Oligomeric state and stability of hDAAO holoenzyme

Gel-permeation chromatography experiments showed that native hDAAO is a dimeric holoenzyme in the 1–24 mg protein/ml concentration range. The oligomerization state of the holoenzyme form of hDAAO is similar to that of the yeast DAAO and is significantly different to that of the closely related pkDAAO [6,19], for which the oligomerization state depends on the protein concentration. hDAAO shows a good stability to urea denaturation (following the 220-nm CD signal a C_m of 4.80 ± 0.15 M was determined, see Fig. 2) and to temperature unfolding (T_m = 52 °C).

3.3. FAD binding

hDAAO contains one molecule of non-covalently bound FAD per protein monomer, which can be easily isolated from the apoprotein by dialysis in the presence of 1 M KBr (with a 70% yield in terms of protein recovered). From changes in fluorescence intensity during the titration of the apoprotein with FAD and from activity assays in the absence and in the presence of exogenous FAD, a K_d of $8 \pm 2 \times 10^{-6}$ M was estimated. Such a value is in good agreement with the value determined previously [10] and significantly higher than the one measured for any other known DAAO (in the 10^{-7}–10^{-8} M range, see Table 1), raising the question of the amount of active hDAAO present in vivo. Interestingly, in the presence of a classical DAAO ligand such as 1 mM benzoate and under the same experimental conditions, the K_d for FAD binding is significantly lower ($=3 \pm 1 \times 10^{-7}$ M) and similar to that of pkDAAO [19].

A further main difference compared to known DAAOs is evident during gel-permeation chromatography: the apoprotein form of the human flavoprotein elutes as a single peak corresponding to a dimeric state while the apoprotein forms of both pk- and RgDAAO are stable 40-kDa monomers [16,19]. This indicates conservation of a large part of the dimerization interface in the apoprotein form. In fact, the hDAAO apoprotein maintains the secondary structure of the holoenzyme (similar far-UV CD spectrum), while some changes are evident in the near-UV CD spectrum, suggesting alteration of the tertiary structure following FAD release (data not shown).

3.4. Substrate specificity

The apparent kinetic parameters on D-serine, the putative "physiological" substrate of hDAAO, determined at 25 °C and 21% oxygen saturation, indicates that hDAAO possesses a low catalytic efficiency and substrate affinity ($k_{cat,app}$ = 3 s^{-1} and $K_{m,app}$ = 7.5 mM). Interestingly, a higher activity was determined on D-alanine and on D-proline (Table 2). Even D-aspartate can be oxidized by hDAAO, but the affinity for this substrate is very low ($K_{m,app} \approx 2$ M). The kinetic

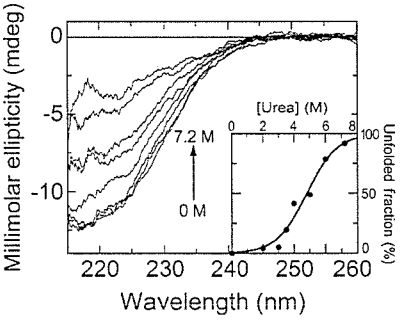

Fig. 2. Effect of urea on hDAAO conformation. CD spectra were recorded after the addition of increasing urea concentration (0–7.2 M); each spectrum was determined on individual sample prepared by mixing appropriate volumes of protein (0.1 mg protein/ml), 8 M urea in buffer, and plain buffer (50 mM sodium pyrophosphate, pH 8.3), at 15 °C. Inset: equilibrium denaturation curve from the CD signal at 220 nm.

parameters determined on D-alanine and D-serine are on the same order of magnitude as those determined for pkDAAO (Table 2) and do not explain how the human enzyme could efficiently bind and oxidize D-serine in vivo (its concentration ranging from 10 to 300 nmol/g wet weight in peripheral tissues and brain, respectively) [2]. Furthermore, even glycine (a neurotransmitter that binds to NMDA receptors in a manner similar to that of D-serine) is oxidized by hDAAO, but with a significantly lower efficiency (Table 2), whereas no activity is evident using NMDA as substrate.

3.5. Kinetic mechanism

The kinetic mechanism of hDAAO was investigated both by the enzyme monitored turnover method as a function of oxygen concentration using D-alanine and D-serine as substrates and by rapid kinetic measurements. Steady-state measurements were performed by mixing the oxidized enzyme aerobically with D-alanine (0.75–5 mM concentration range) or D-serine (1–10 mM concentration range) and monitoring the change in flavin absorption at 455 nm (data not shown). A rapid initial decrease in absorption was observed, amounting to ~10–15% of the total change, followed by a stationary phase, whose duration depended on the initial D-amino acid concentration, and which converted into the fully reduced enzyme as the final state. In all cases, a slow decrease in the absorbance is evident at longer times (due to the binding of the free coenzyme to the apoprotein form present in the solution, see below), and was not considered for calculations. The 455-nm traces were analyzed as a function of oxygen concentration according to [18]. Lineweaver–Burk plots at different substrate concentrations show a set of parallel lines pointing to an apparent ping-pong kinetic mechanism or to formation of a ternary complex with some of the rate constants sufficiently small that the bimolecular term $\Phi_{D\text{-}AA,O_2}$ of the steady-state equation becomes negligible at high substrate concentrations (see Eqs. (1), (2)):

Table 2
Comparison of the substrate specificity of DAAO from different sources

	hDAAO	pkDAAO[a]	RgDAAO[b]
D-Alanine			
$k_{cat,app}$ (s^{-1})	5.2	6.4	85
$K_{m,app}$ (mM)	1.3	3.1	0.8
D-Serine			
$k_{cat,app}$ (s^{-1})	3.0	5.8	40.7[c]
$K_{m,app}$ (mM)	7.5	41	13.7[c]
D-Proline			
$k_{cat,app}$ (s^{-1})	10.2	43.3	77.3
$K_{m,app}$ (mM)	8.5	2	21.5
Glycine			
$k_{cat,app}$ (s^{-1})	0.9	b.d.	9.5[c]
$K_{m,app}$ (mM)	180		160[c]
D-Aspartate			
$k_{cat,app}$ (s^{-1})	6.7	b.d.	0.7
$K_{m,app}$ (mM)	2000		33.1

The apparent kinetic parameters were determined by the oxygen-consumption assay at 21% oxygen saturation, pH 8.5 and at 25 °C.
b.d., below detection.
[a]Ref. [21].
[b]Ref. [22].
[c]Unpublished results.

$$e_t/v = \Phi_0 + \Phi_{D\text{-}Ala}/[D\text{-}AA] + \Phi_{O2}/[O_2] + \Phi_{D\text{-}AA,O_2}/[D\text{-}AA][O_2], \quad (1)$$

where $k_{cat} = 1/\Phi_0$; $K_{m,D\text{-}AA} = \Phi_{D\text{-}AA}/\Phi_0$; $K_{m,O_2} = \Phi_{O_2}/\Phi_0$.

$$\frac{e_t}{v} = \frac{k_2 + k_4}{k_2 \cdot k_4} + \frac{k_{-1} + k_2}{k_1 \cdot k_2[D\text{-}AA]} + \frac{k_2 + k_{-2}}{k_2 \cdot k_3[O_2]} + \frac{k_{-1} + k_{-2}}{k_1 \cdot k_2 \cdot k_3[D\text{-}AA][O_2]}. \quad (2)$$

The steady-state coefficients confirm the low activity and substrate affinity of hDAAO obtained at fixed oxygen concentration (see Tables 2 and 3).

For reductive half-reaction experiments, ~10 μM of enzyme was anaerobically mixed with different concentrations of D-amino acid in the stopped-flow instrument: the time course of flavin reduction at 455 nm shows three phases and the one at 530 nm shows two phases (Fig. 3). This behavior is due to two different processes: the reduction of the flavin bound to the enzyme (first and second phase, Eq. (3a)) and the reduction of the flavin following the slow binding of the free coenzyme to the hDAAO apoprotein (third phase, Eq. (3b)):

$$E\text{-}FAD_{ox} + D\text{-}AA \underset{k_{-1}}{\overset{k_1}{\rightleftarrows}} E\text{-}FAD_{ox} : D\text{-}AA \underset{k_{-2}}{\overset{k_2}{\rightleftarrows}} E\text{-}FAD_{red} : IA \underset{k_{-3}}{\overset{k_3}{\rightleftarrows}} E\text{-}FAD_{red} + IA \quad (3a)$$

$$Apoprotein + FAD_{ox} \underset{k_{off}}{\overset{k_{on}}{\rightleftarrows}} E\text{-}FAD_{ox} \quad (3b)$$

In fact, using a 10 μM enzyme solution (and because of the weak binding of the flavin cofactor to hDAAO) about 40% of the enzyme is in the apoprotein form: this value nicely corresponds to the amplitude of the third phase on the entire absorbance change at 455 nm (see Fig. 3). The observed rate constants of the first (rapid) phase exhibited saturation with increasing D-amino acid concentration, while the second and the third phase were insensitive to substrate concentration. The first phase corresponds to the flavin reduction yielding a charge-transfer complex between the reduced enzyme and the product imino acid (IA) having a broad absorbance peak centered at ~530 nm (see Eq. (3a) and spectrum 3 in Fig. 3 inset). Analogously to pk- and RgDAAO [17,20], steps k_1 and k_{-1} were not observed spectrophotometrically, implying that substrate binding did not affect the oxidized flavin chromophore to a measurable extent. Interestingly, the rate of flavin reduction (k_2) is significantly faster than the turnover number (see Table 3), i.e., it is not rate limiting in catalysis. The second phase corresponds to the imino acid release from the reduced enzyme form ($k_3 \sim 0.6$–$0.9\ s^{-1}$) yielding the free reduced enzyme (spectrum 4 in Fig. 3 inset). We replicated the experimental spectral time courses with Specfit/32 software (Fig. 3): the simulations confirm the values of the aforementioned kinetic parameters and allowed to estimate the minimal values of k_1 and k_{-1} ($=1.5 \pm 0.5 \times 10^4\ M^{-1}\ s^{-1}$ and $100 \pm 20\ s^{-1}$, respectively). The same simulations confirm that the third phase corresponds to the slow flavin reduction following the binding of the free oxidized FAD (spectrum 2 in Fig. 3 inset) to the apoprotein form present in the assay mixture ($k \sim 0.01\ s^{-1}$, Eq. (3b)).

For reoxidation experiments, the enzyme was first reduced with a small excess (2- or 3-fold) of substrate under anaerobic conditions. The oxidative half-reaction was initially investigated by reacting the free reduced form of hDAAO with buffer

Table 3
Comparison of the steady-state coefficients, reductive and oxidative half-reaction specific rate constants of hDAAO, pkDAAO and RgDAAO on D-alanine as substrate determined by rapid mixing techniques [17] at pH 8.3 and 25 °C

	hDAAO	pkDAAO[a]	RgDAAO[b]
Steady-state			
Lineweaver–Burk plot	Parallel	Parallel	Parallel
k_{cat} (s^{-1})	14.7 ± 0.7 (6.3 ± 1.4)	10	350
$K_{m,D\text{-}Ala}$ (mM)	8.8 ± 0.3 (19.8 ± 3.4)	2.0	2.6
K_{m,O_2} (mM)	1.2 ± 0.3 (2.2 ± 0.7)	0.15	2.3
$\Phi_{D\text{-}Ala}$ ($M\,s \times 10^{-3}$)	0.6 ± 0.1 (3.2 ± 0.7)	0.2	0.0074
Φ_{O_2} ($M\,s \times 10^{-5}$)	8 ± 0.3 (0.35 ± 0.1)	1.5	0.0065
Reductive half-reaction			
k_2 (s^{-1})	180 ± 20 (117 ± 6)	4000	345
K_{d,app_1} (mM)	12.7 ± 2.8 (34.5 ± 3.2)	420	2.8
k_3 (s^{-1})	0.6 ± 0.2 (0.9 ± 0.3)	0.02	2.8
Oxidative half-reaction			
k_4 ($M^{-1}\,s^{-1}$) × 10^4	1.7 ± 0.6	4.6	4.6
k_5 ($M^{-1}\,s^{-1}$) × 10^4	12.5 ± 4.2	17	11

The $K_{d,app}$ was obtained from the slope divided by the intercept in the double-reciprocal plot of the rate of reduction vs. D-amino acid concentration. The values determined on D-serine as substrate are shown in parentheses. For hDAAO and pkDAAO k_{cat} corresponds to k_6, while for RgDAAO the rate limiting step in catalysis is k_2 (see Fig. 4).
[a]Ref. [20].
[b]Ref. [17].

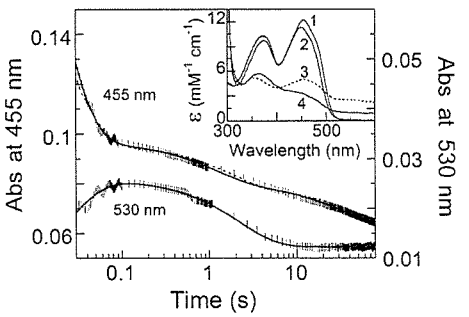

Fig. 3. Time course of the anaerobic reduction of ~10.4 μM hDAAO by 5 mM D-alanine followed at 455 nm and 530 nm (|). Curve (—) is the fit for a triple (trace at 455 nm) or a double (trace at 530 nm) exponential decay; curve (---) is the trace obtained from simulation using the Specfit/32 software and based on the sequence of steps of Eqs. (3a) and (3b), on spectra of colored species (see inset), and on the rate constants reported in Table 3 and in the text (k_1 = $1.5 \times 10^4\ M^{-1}\,s^{-1}$, $k_{-1} = 100\ s^{-1}$, $k_{-2} = 0.01\ s^{-1}$, and $k_{-3} \sim 0$). Inset: the spectra shown are those of the known oxidized hDAAO (1) and oxidized free FAD (2), and those obtained by deconvolution of the experimental data with Specfit/32 using a model according to the sequence of steps reported in Eqs. (3a) and (3b): spectrum (3, —) corresponds to the intermediate identified during the enzyme reduction process (reduced enzyme ~ IA complex) and spectrum (4) is that of the free reduced enzyme. Minor differences between the identified spectra and the real ones depend on the presence of free FAD in the solution (and because of the low K_d for coenzyme binding of hDAAO).

solutions equilibrated at increasing oxygen concentration (Eq. (4a)): spectra were recorded during flavin reoxidation (data not shown). The time course of absorbance change at 455 nm was monophasic and the observed rates depended linearly on oxygen concentration and were extrapolated to the origin, consistent with a second-order reaction in dioxygen. A reoxidation rate constant of $1.7 \pm 0.6 \times 10^4\ M^{-1}\,s^{-1}$ was calculated (Table 3). Subsequently, the rate of reoxidation of reduced enzyme bound to the final product imino acid was investigated. Unfortunately, a reduced enzyme–imino acid complex cannot be produced experimentally as it hydrolyzes in the presence of water. Since this compound is unstable in aqueous solution, we tried to produce it by adding pyruvate and ammonium chloride to the enzyme solution (analogously to that previously performed for RgDAAO) [17]. The anaerobic titration of fully reduced hDAAO using increasing concentrations of pyruvate in the presence of 0.4 M ammonium chloride yielded the oxidized enzyme form. This result demonstrates that the reductive half-reaction is reversible (k_{-2} in Eq. (3a) is small but it is different from zero). In order to produce a significant percentage of the E-FAD_{red}:IA complex in the reaction mixture, the reoxidation reaction was performed with buffer containing 0.4 M ammonium chloride and 20 or 50 mM pyruvate. Under these conditions the absorbance increase at 455 nm was biphasic (data not shown). The amplitude of the absorbance change associated to each single phase does not depend on the oxygen concentration, but it is largely dependent on the pyruvate concentration (the absorbance change associated to the fast phase corresponded to ~50% of the total change at 20 mM pyruvate and ~70% at 50 mM pyruvate). Both the observed rates depended on the oxygen concentration. Our interpretation of this finding is represented by Eq. (4): we assume that the E-FAD_{red} and the E-FAD_{red}:IA forms are in rapid equilibrium and therefore that the reoxidation can start from both the free (Eq. (4a)) and the IA-complexed form (Eq. (4b)) of the reduced enzyme:

$$k_4 \approx 1 \times 10^4\ M^{-1}s^{-1}$$

$$\text{E-FAD}_{red} + O_2 \quad \text{(a)} \qquad \text{E-FAD}_{ox} + H_2O_2 \quad (4)$$

$$k_5 = 1.2 \times 10^5\ M^{-1}s^{-1}$$

$$\text{E-FAD}_{red}\text{:IA} + O_2 \qquad \text{IA} \quad \text{(b)}$$

The reoxidation rate of the slow phase is in good agreement with the value determined in the absence of pyruvate

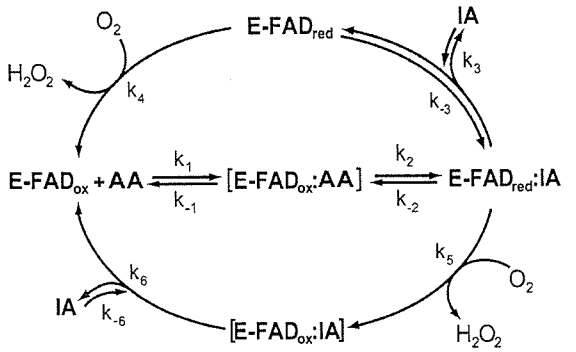

Fig. 4. Kinetic scheme of the reaction of hDAAO. Lower loop: ternary complex mechanism; upper loop: ping-pong mechanism. The species not detected spectrophotometrically, but which were required by the kinetic mechanism, are shown in parenthesis.

($=1.7 \pm 0.6 \times 10^4\ M^{-1}\ s^{-1}$). On the other hand, the second-order rate constant for the first (rapid) phase is significantly faster: $k_5 = 1.2 \pm 0.4 \times 10^5\ M^{-1}\ s^{-1}$. This model of the oxidative half-reaction was validated by simulation of the spectral time courses using Specfit/32 software: a good simulation was only obtained when a 1:1 and 1:2 ratio between E-FAD_{red} and E-FAD_{red}:IA forms was used at 20 and 50 mM pyruvate, respectively, which is in good agreement with the absorbance change associated to the two phases (see above).

The combination of steady-state and pre-steady-state measurements (see Table 3) indicates that: (i) hDAAO follows a tertiary complex (sequential) kinetic mechanism (lower loop of Fig. 4) since k_3 is too slow to belong to the turnover kinetic mechanism. This mechanism is similar to that observed with pk- and RgDAAO with neutral substrates [17,20]; (ii) the kinetic parameters are on the same order of magnitude as those determined for pkDAAO (the main difference is represented by the rate of flavin reduction, which is 20-fold slower in the human enzyme, see Tables 2 and 3); and (iii) the rate of product release from the reoxidized enzyme form (k_6) is the rate-limiting step in catalysis, analogous to that observed for pkDAAO [20].

4. Conclusions

In this work we reported on the expression of fairly large amounts of hDAAO, a stable and active holoenzyme. This human enzyme shows the classical properties of the dehydrogenase-oxidase class of flavoproteins (it reacts quickly with oxygen in the reduced state, stabilizes the anionic red semiquinone, and binds sulfite covalently) and shares these properties with both pk- and RgDAAO [6,19]. On the other hand, hDAAO possesses some peculiar properties. In particular, binding of the FAD cofactor to the human enzyme in the absence of an active site ligand is the weakest among known DAAOs, and it is also the only DAAO apoprotein present in solution as a dimer. From the kinetic point of view, hDAAO shows the same rate limiting step (represented by the product release from the reoxidized enzyme) and the same sequential mechanism reported for pkDAAO on neutral D-amino acids, but a significant slower rate of flavin reduction [20]. In comparison to the yeast DAAO, and even if the two enzymes shows the same kinetic mechanism, hDAAO possesses a different rate limiting step in catalysis and a ~10-fold lower activity [6,17]. These results contribute to further elucidating the effect of the inferred binding protein pLG72 on the stability and kinetics of the reaction catalyzed by DAAO in human brain with the aim of designing specific drugs that could alter the properties of this key enzyme in glutamatergic neurotransmission.

Acknowledgements: This work was supported by Grants from Italian MIUR to M.S. Pilone (Prot. 2004058243), from FAR to M.S. Pilone and L. Pollegioni, and from Fondazione CARIPLO to L. Pollegioni.

References

[1] Krebs, H.A. (1935) Metabolism of amino-acids. III. Deamination of amino-acids. Biochem. J. 29, 1620–1644.
[2] Hashimoto, A. and Oka, T. (1997) Free D-aspartate and D-serine in the mammalian brain and periphery. Progr. Neurobiol. 52, 325–353.
[3] Mothet, J.P., Parent, A.T., Wolosker, H., Brady Jr., R.O., Linden, D.J., Ferris, C.D., Rogawski, M.A. and Snyder, S.H.. (2000) D-Serine is an endogenous ligand for the glycine site of the *N*-methyl-D-aspartate receptor. Proc. Natl. Acad. Sci. USA 97, 4926–4931.
[4] Chumakov, I. et al. (2002) Genetic and physiological data implicating the new human gene G72 and the gene for D-amino acid oxidase in schizophrenia. Proc. Natl. Acad. Sci. USA 99, 13675–13680.
[5] Molla, G., Bernasconi, M., Sacchi, S., Pilone, M.S. and Pollegioni, L. (2006) Expression in *Escherichia coli* and in vitro refolding of the human protein pLG72. Protein Expr. Purif. 46, 150–155.
[6] Pilone, M.S. (2000) D-Amino acid oxidase: new findings. Cell. Mol. Life Sci. 57, 1732–1747.
[7] Mattevi, A., Vanoni, M.A., Todone, F., Rizzi, M., Teplyakov, A., Coda, A., Bolognesi, M. and Curti, B. (1996) Crystal structure of D-amino acid oxidase: a case of active site mirror-image convergent evolution with flavocytochrome b2. Proc. Natl. Acad. Sci. USA 93, 7496–7501.
[8] Umhau, S., Pollegioni, L., Molla, G., Diederichs, K., Welte, W., Pilone, M.S. and Ghisla, S. (2000) The X-ray structure of D-amino acid oxidase at very high resolution identifies the chemical mechanism of flavin-dependent substrate dehydrogenation. Proc. Natl. Acad. Sci. USA 97, 12463–12468.
[9] Momoi, K., Fukui, K., Watanabe, F. and Miyake, Y. (1988) Molecular cloning and sequence analysis of cDNA encoding human kidney D-amino acid oxidase. FEBS Lett. 238, 180–184.
[10] Raibekas, A.A., Fukui, K. and Massey, V. (2000) Design and properties of human D-amino acid oxidase with covalently attached flavin. Proc. Natl. Acad. Sci. USA 97, 3089–3093.
[11] Molla, G., Vegezzi, C., Pilone, M.S. and Pollegioni, L. (1998) Overexpression in *Escherichia coli* of a recombinant chimeric *Rhodotorula gracilis* D-amino acid oxidase. Protein Expr. Purif. 14, 289–294.
[12] Massey, V. and Hemmerich, P. (1978) Photoreduction of flavoproteins and other biological compounds catalyzed by deazaflavins. Biochemistry 17, 9–16.
[13] Massey, V. (1991) A simple method for the determination of redox potentials Flavins and Flavoproteins, pp. 59–66, Walter de Gruyter & Co., Berlin.
[14] Pollegioni, L., Porrini, D., Molla, G. and Pilone, M.S. (2000) Redox potentials and their pH dependence of D-amino acid oxidase of *Rhodotorula gracilis* and *Trigonopsis variabilis*. Eur. J. Biochem. 267, 6624–6632.
[15] Minnaert, K. (1965) Measurement of the equilibrium constant of the reaction between cytochrome *c* and cytochrome *a*. Biochim. Biophys. Acta 110, 42–56.
[16] Casalin, P., Pollegioni, L., Curti, B. and Pilone, M.S. (1991) A study on apoenzyme from *Rhodotorula gracilis* D-amino acid oxidase. Eur. J. Biochem. 197, 513–517.

[17] Pollegioni, L., Langkau, B., Tischer, W., Ghisla, S. and Pilone, M.S. (1993) Kinetic mechanism of D-amino acid oxidase from *Rhodotorula gracilis* and *Trigonopsis variabilis*. J. Biol. Chem. 268, 13850–13857.
[18] Gibson, Q.H., Swoboda, B.E.P. and Massey, V. (1964) Kinetics and mechanism of action of glucose oxidase. J. Biol. Chem. 259, 3927–3934.
[19] Curti, B., Ronchi, S. and Pilone Simonetta, M. (1992) D- and L-amino acid oxidases in: (Müller, F., Ed.), Chemistry and Biochemistry of Flavoenzymes, vol. III, pp. 69–94, CRC Press, Boca Raton.
[20] Porter, D.J.T., Voet, J.G. and Bright, H.J. (1977) Mechanistic features of the D-amino acid oxidase reaction studied by double stopped flow spectrophotometry. J. Biol. Chem. 252, 4464–4473.
[21] Dixon, M. and Kleppe, K. (1965) D-Amino acid oxidase. II: Specificity, competitive inhibition and reaction sequence. Biochim. Biophys. Acta 96, 368–382.
[22] Sacchi, S., Lorenzi, S., Molla, G., Pilone, M.S., Rossetti, C. and Pollegioni, L. (2002) Engineering the substrate specificity of D-amino-acid oxidase. J. Biol. Chem. 277, 27510–27516.

Journal of Neurochemistry, 2006, **97**, 1126–1135 doi:10.1111/j.1471-4159.2006.03833.x

Attenuation of MPTP-induced neurotoxicity and locomotor dysfunction in Nucling-deficient mice via suppression of the apoptosome pathway

Xichuan Teng,* Takashi Sakai,* Li Liu,* Rika Sakai,*,† Ryuji Kaji† and Kiyoshi Fukui*

**The Institute for Enzyme Research, The University of Tokushima, Tokushima, Japan*

†Department of Neurology, Tokushima University School of Medicine, Tokushima, Japan

Abstract

1-Methyl-4-phenyl-1,2,3,6-tetrahydropyridine (MPTP)-induced neurotoxicity is one of the experimental models most commonly used to study the pathogenesis of Parkinson's disease (PD). Although the biochemical mechanisms underlying the cell death induced by MPTP remain to be clarified, it has been found that the mitochondrial apoptotic signaling pathway plays an important role in the neurotoxicity of MPTP. Nucling is a novel type of apoptosis-associated molecule, essential for cytochrome *c*, apoptosis protease activating factor 1 (Apaf-1), procaspase-9 apoptosome induction and caspase-9 activation following pro-apoptotic stress. Here we found that Nucling-deficient mice treated with MPTP did not exhibit locomotor dysfunction in an open-field test. The substantia nigra dopaminergic neurons of Nucling-deficient mice were resistant to the damaging effects of the neurotoxin MPTP. Up-regulated expression of apoptosome was attenuated in Nucling-deficient mice treated with MPTP. These results indicate an important role for Nucling in MPTP-induced neuronal degeneration and suggest that the suppression of Nucling would be of therapeutic benefit for the treatment of neurodegeneration in PD.

Keywords: apoptosis, apoptosome, MPTP, Nucling, Parkinson's disease.

J. Neurochem. (2006) **97**, 1126–1135.

Parkinson's disease (PD) is a progressive disorder resulting from the degeneration of dopaminergic neurons in the substantia nigra (SN). The clinical manifestations of PD include resting tremors, rigidity, slowness of movement and postural instability (Kopin and Markey 1988). Except for a handful of inherited cases related to known gene defects, PD is a sporadic condition of unknown pathogenesis. Although the actual cause of PD remains unknown, the dying neurons of the Parkinsonian brain display morphological characteristics of apoptosis (Mochizuki *et al.* 1996; Hajimohamadreza and Treherne 1997; Tatton *et al.* 1998). Recently, significant insights into the pathogenesis of PD have been yielded by the use of 1-methyl-4-phenyl-1,2,3,6-tetrahydropyridine (MPTP), a neurotoxin. Systemic administration of MPTP produces behavioral changes and neuropathological hallmarks similar to those of PD (Chiueh *et al.* 1984; Heikkila *et al.* 1984; Langston 1996). After its administration, MPTP is transformed to the 1-methyl-4-phenylpyridium cation (MPP^+) by monoamine oxidase type B (MAOB), and then is selectively taken up by the dopaminergic neurons in the SN via the dopamine transporter. MPP^+ accumulates in the mitochondria (Mizuno *et al.* 1987; Langston 1996), where it selectively inhibits complex I of the electron transport chain, thereby blocking the production of ATP (Nicklas *et al.* 1985; Mizuno *et al.* 1995; Przedborski and Jackson-Lewis 1998).

Although the MPTP-induced death of dopaminergic neurons is well recognized, its pathogenesis is poorly understood. Recently, the mitochondrial apoptotic cascade has been shown to play an important role in the neurotoxicity

Received September 21, 2005; revised manuscript received January 27, 2006; accepted January 27, 2006.

Address correspondence and reprint requests to Kiyoshi Fukui, The Institute for Enzyme Research, The University of Tokushima, 3-18-15 Kuramoto-Cho, Tokushima, 770–8503, Japan.
E-mail: kiyo@ier.tokushima-u.ac.jp

Abbreviations used: Apaf-1, apoptosis protease activating factor 1; GAPDH, glyceraldehyde-3-phosphate dehydrogenase; MEF, murine embryonic fibroblast; MPP^+, 1-methyl-4-phenylpyridinium; MTP, mitochondrial transition pore; MPTP, 1-methyl-4-phenyl-1,2,3,6-tetrahydropyridine; Nucl. mid., the middle portion of Nucling; PBS, phosphate-buffered saline; PD, Parkinson's disease; SN, substantia nigra; SNpc, substantia nigra pars compacta; TH, tyrosine hydroxylase; TUNEL, terminal deoxynucleotidyl transferase-mediated dUTP nick-end labeling; WT, wild-type.

of MPTP (Mochizuki *et al.* 2001; Viswanath *et al.* 2001). In addition, the expression of characteristic components of the mitochondrial apoptotic cascade, including cytochrome *c* and caspase-9, was up-regulated in SN tissue isolated from mice treated with MPTP (Viswanath *et al.* 2001). Transgenic mice that neuronally express p35, a potent irreversible caspase inhibitor, have been shown to be resistant to MPTP-induced dopaminergic neuronal loss (Viswanath *et al.* 2001). On the other hand, mice overexpressing the anti-apoptotic protein Bcl-2 in the brain were insensitive to MPTP-induced neurotoxicity (Yang *et al.* 1998). Several caspase inhibitors, such as the peptidyl inhibitor Q-VD-OPH, can protect tyrosine hydroxylase (TH)-positive neurons from apoptotic death caused by MPTP (Yang *et al.* 2004). Therefore, the mitochondrial apoptotic cascade has been suggested to be crucial in MPTP-induced dopaminergic neurotoxicity.

Nucling is a novel apoptosis-associated protein isolated from murine embryonal carcinoma cells (Sakai *et al.* 2003). Recently, we reported that the expression of Nucling was up-regulated in response to pro-apoptotic stimuli, and that overexpressed Nucling was able to induce apoptosis *in vitro*. In addition, we have confirmed that Nucling was essential for the cytochrome *c*, apoptosis protease activating factor 1 (Apaf-1), caspase-9 apoptosome induction and caspase-9 activation following pro-apoptotic stress. Furthermore, in Nucling-deficient murine embryonic fibroblast (MEF) cells, the expression of both Apaf-1 and cytochrome *c* was down-regulated under cellular stress, and Nucling-deficient cells were resistant to cytotoxic stress (Sakai *et al.* 2003, 2004).

In this report, we show that Nucling is involved in MPTP-induced neurotoxicity. The expression of Nucling in SN was up-regulated after the administration of MPTP. MPTP-induced dopaminergic neuronal damage and locomotor dysfunction were attenuated in Nucling-deficient mice. Moreover, in the SN, the up-regulation of the apoptosome and the activation of caspase-9 induced by MPTP were suppressed in Nucling-deficient mice. These findings suggest that Nucling acts as an important factor during MPTP-induced apoptosis of SN dopaminergic neurons through the activation of the mitochondrial apoptotic cascade.

Materials and methods

MPTP treatment of mice

C57BL/6 mice (8–12 weeks of age) were used. Nucling-deficient mice were generated by gene-targeting techniques and back-crossed for eight generations into the C57BL/6 background (Sakai *et al.* 2004). MPTP-HCl (Sigma, St Louis, MO, USA) in phosphate-buffered saline (PBS) (–) was administered to wild-type (WT) and Nucling-deficient male mice, using an acute dosing regimen of 15 mg/kg administered intraperitoneally every 2 h for four doses. Control animals in both paradigms were treated with equal volumes of PBS (–).

RT–PCR

Total RNA from the ventral midbrain of either PBS (–)- or MPTP-injected WT and Nucling-deficient mice was prepared using ISOGEN (Nippon Gene, Tokyo, Japan). The concentration and purity of the RNA preparations were determined by measuring the absorbance at 260 and 280 nm in a spectrophotometer. RT was performed using 1 μg of total RNA (at 42°C for 2 h) in a 20-μL reaction volume containing oligo(dT) primer and Superscript II reverse transcriptase (Invitrogen, Carlsbad, CA, USA). The PCR primers, the designs of which were based on the published cDNA sequences of Nucling, were 5′-TGATCACCCAGGACCCGGAAG-TTACC-3′ (sense) and 5′-GGTGCTCTTTGAGGGCGAGGAAG-TG-3′ (anti-sense). The PCR program consisted of 34 cycles of 95°C for 1 min, 60°C for 1 min and 72°C for 2 min. PCR products were analyzed on 1.2% agarose gel. RT–PCR of glyceraldehyde-3-phosphate dehydrogenase (GAPDH) was used as a control.

Western blot analysis

At the indicated time points after treatment, ventral midbrain was quickly dissected and lysed in lysis buffer [0.21 M mannitol, 70 mM sucrose, 10 mM HEPES–KOH, pH 7.2, 1 mM EDTA, 1 mM EGTA, 0.15 mM spermine, 0.75 mM spermidine and 5 mM dithiothreitol (DTT) plus 2 μg/mL leupeptin, 2 μM benzamidine-HCl and 1 μg/mL pepstatin] (Viswanath *et al.* 2001). Nuclei and unlysed cells were removed by centrifugation at 500 *g* for 12 min at 4°C. The supernatant was centrifuged at 9500 *g* for 9 min at 4°C to pellet mitochondria. The supernatant contained the cytosolic fraction. Antibodies reactive to cytochrome *c* (dilution 1 : 400; BML, Nagoya, Japan), Apaf-1 (dilution 1 : 1000; Chemicon, Temecula, CA, USA), caspase-9 (dilution 1 : 1000; Cell Signaling, Beverly, MA, USA), β-tubulin (dilution 1 : 2000; Sigma, St Louis, MO, USA), and the middle portion of Nucling (Nucl. Mid.) (Sakai *et al.* 2004) were used in this study. Western blot analysis was carried out according to standard procedures using an ECL detection kit (Amersham Biosciences, Buckinghamshire, UK).

Immunohistochemistry

At the indicated time point, mice were perfused via the intracardiac route with PBS, followed by 4% paraformaldehyde in PBS. The brains were removed and immersed for 48 h in 4% paraformaldehyde for fixation. Forebrain and nigral sections (6 μm) were prepared with a sliding microtome. Sections were immunostained with a mouse monoclonal anti-TH (dilution 1 : 400; Chemicon) for striatal fibers and dopaminergic neurons overnight at 4°C. The sections were then washed with PBS and incubated with biotinylated secondary antibody, rinsed and placed for 30 min in avidin-biotin peroxidase solution (ABC elite kit; Vector Laboratories, Burlingame, CA, USA). Finally, sections were incubated with diaminobenzidine (DAB) for visualization.

For the quantification of dopaminergic neurons in the midbrain of WT and Nucling-deficient mice, we counted all TH-positive neurons of one hemisphere from 20 coronal sections (10 μm) from each mouse ($n = 3$ per group). Sections were distributed every 50 μm along the rostral-caudal axis of the SN (from −2.7 mm to −3.8 mm between caudal and bregma). The neuronal diameter was considered to be 20 μm (Nelson *et al.* 1996). Abercrombie's correction was used to estimate the average number of neurons per section according to the formula $N = n \times T/(T + D)$, where N = number,